IgA-driven neutrophil activation underlies post-Zika severe dengue disease in humans

Authors:

Jaime A. Cardona-Ospina[1,2], Vicky Roy[3], Dorca E. Marcano-Jiménez[4], Sandra Bos[1], Elias Duarte[1], José V. Zambrana[5,6], Agamjot Bal[1], Boyeong K. An[1], Antonio Gregorio Dias Jr.[1], Julia Zhiteneva[3], Julia Huffaker[1], Carlos Montenegro[5], Guillermina Kuan[5,7], Marcos J. Ramos-Benitez[4], Angel Balmaseda[5,8], Galit Alter[3], Eva Harris[1]*

Affiliations:

[1]Division of Infectious Diseases and Vaccinology, School of Public Health, University of California, Berkeley, Berkeley, CA

[2]Grupo Biomedicina, Facultad de Medicina, Institución Universitaria Visión de las Américas, Pereira, Colombia

[3]Ragon Institute of MGH, MIT, and Harvard, Cambridge, MA

[4]Department of Basic Sciences, Ponce Health Sciences University and Ponce Research Institute, Ponce, Puerto Rico

[5]Sustainable Sciences Institute, Managua, Nicaragua

[6]Department of Epidemiology, School of Public Health, University of Michigan, Ann Arbor, MI

[7]Centro de Salud Sócrates Flores Vivas, Ministerio de Salud, Managua, Nicaragua

[8]Laboratorio Nacional de Virología, Centro Nacional de Diagnóstico y Referencia, Ministerio de Salud, Managua, Nicaragua

*Corresponding author. Email: eharris@berkeley.edu

Abstract

The four dengue virus serotypes (DENV1-4) and the related Zika flavivirus (ZIKV) are major public health concerns worldwide. Primary immunity against ZIKV increases the risk of a subsequent severe DENV2 infection, presenting a significant challenge for developing safe and effective ZIKV vaccines. However, the mechanisms driving this phenomenon remain unclear. Leveraging our long-standing Pediatric Dengue Cohort Study in Nicaragua, we show that serum anti-NS1 IgA antibodies elicited after a primary ZIKV infection drive neutrophil activation and correlate with increased risk of subsequent severe DENV2 disease. Depletion experiments combined with e*x vivo* functional NETosis assays confirmed that anti-NS1 IgA antibodies drive neutrophil activation in dengue hemorrhagic fever/dengue shock syndrome (DHF/DSS). Moreover, increased neutrophil degranulation in paired serum samples obtained during the acute DENV2 infection from the same individuals correlated with IgA binding to DENV2 NS1 and preceded the development of vascular leakage. This finding was corroborated in an orthogonal hospital-based study. Thus, serum anti-NS1 IgA enhances neutrophil activation in severe dengue, with implications for prognostics, therapeutics, and vaccines.

Main Text

The four serotypes of dengue virus (DENV1-4) and Zika virus (ZIKV) are closely related flaviviruses that co-circulate and constitute the most prevalent causes of arboviral disease globally [1]. DENV infections exhibit a clinical spectrum ranging from a self-limited febrile illness (dengue fever [DF]) to more severe, potentially fatal forms such as dengue hemorrhagic fever and dengue shock syndrome (DHF/DSS) characterized by thrombocytopenia, vascular leakage, and hemorrhagic manifestations[2]. Sequential infections with different DENV serotypes or ZIKV can either confer protection or increase the risk of subsequent severe disease[3–6]. This phenomenon, primarily driven by the humoral immune response, presents significant challenges for the development of safe and effective vaccines.

During sequential DENV infections, sub-neutralizing cross-reactive IgG antibodies targeting structural viral proteins can facilitate viral entry into myeloid cells expressing Fcγ receptors, increasing viral load through a phenomenon known as antibody-dependent enhancement (ADE)[7,8]. In addition, afucosylated IgG antibodies generated during the acute secondary infection further enhance disease severity by promoting cellular activation via FcγRIIIA[9,10]. Epidemiological studies have shown that a primary ZIKV infection increases the likelihood of subsequent symptomatic DENV infections and severe disease[4,5]. This association is strongly correlated with antibody levels, as a specific range of ZIKV-induced DENV cross-reactive antibodies are linked to an elevated risk of severe outcomes upon a subsequent DENV infection[4]. Therefore, understanding antibody features that underlie increased risk is essential for developing safe and effective vaccines.

To explore this, we employed an agnostic systems serology approach to characterize DENV cross-reactive antibodies after a prior ZIKV infection and before a subsequent symptomatic infection with DENV2, leveraging unique serum samples from our long-standing Pediatric Dengue Cohort Study (PDCS) in Nicaragua[11]. Our findings reveal that pre-existing IgA antibodies, particularly those targeting the nonstructural protein 1 (NS1), are key predictive features of DHF/DSS. Using systems serology and functional assays in paired pre-infection and acute-phase samples from the same individuals, we provide novel insights into the role of anti-NS1 IgA antibodies in mediating heightened neutrophil activation, a characteristic of children that progressed to severe disease. This insight reveals a previously unappreciated mechanism of IgA-mediated neutrophil activation in dengue disease that may underpin progression to severe disease

in sequential flavivirus infections. These results have broad implications for understanding immune responses against flaviviruses in co-endemic regions and informing vaccine development. Moreover, they highlight the potential role of serum IgA antibodies in mediating neutrophil-mediated pathogenesis in infectious diseases.

Results

Pre-existing IgA antibodies differentiate severe and non-severe DENV infections

A prior ZIKV infection increases the risk of both symptomatic and severe disease during a subsequent DENV infection[4–6]. While this elevated risk has been linked to DENV cross-reactive antibodies induced by ZIKV[4], the specific characteristics of these antibodies remain undefined. To address this gap, we employed an agnostic systems serology approach to evaluate the antigenic targets and isotypes of pre-existing antibodies associated with increased risk of DHF/DSS.

Our analysis focused initially on serum samples collected after primary ZIKV infection and before subsequent DENV2 infection from 24 children enrolled in the PDCS in Nicaragua. These children experienced a primary ZIKV infection in 2016, followed by a DENV2 infection in 2019–2020, which resulted in either DF (n = 14) or DHF/DSS (n = 10; Fig. 1A). The median time between plasma sample collection and the subsequent DENV2 infection was 7.16 months (interquartile rank (*IQR)*: 6.32–7.97) for individuals who developed DF and 7.84 months (*IQR*: 6.52–8.29) for those who developed DHF/DSS (p=0.7). Using a multiplexed bead-based assay[12], we characterized the antibody binding profile against the envelope protein (E), domain III of E (EDIII), and NS1 of DENV1–4 and ZIKV, evaluating total IgG, IgG1–4, IgM, and IgA antibodies.

After correcting for false discovery rate (FDR), only binding of IgA antibodies differed significantly between the clinical groups across all tested antigens and isotypes (Extended Data Fig. 1A). Additionally, increased ED_{50} values of IgA antibodies, reflecting the dilution at which binding is reduced to 50%, were uniquely associated with an elevated risk of developing DHF/DSS (Fig. 1B). In a regularized multivariate model, IgA binding to NS1 of the incoming serotype (DENV2) emerged as the variable with the highest adjusted coefficient, highlighting its strong association with severe disease outcomes (Fig. 1C).

To further assess the specificity of the IgA immune response, we measured total IgA levels in plasma. Total IgA concentrations were comparable across groups and were within the

102 physiological range (DF: median = 1.2 mg/mL, IQR: 0.6–1.3 mg/mL; DHF/DSS: median = 1.1
103 mg/mL, IQR: 0.9–1.2 mg/mL; p = 0.88), indicating that the observed differences in anti-DENV
104 IgA were not due to overall systemic IgA levels but were instead antigen-specific. We next
105 examined the clinical relevance of this response by comparing children with primary ZIKV
106 infection who subsequently experienced either inapparent (n = 18) or symptomatic (n = 14)
107 DENV2 infection. In pre-infection serum samples, only IgA binding to NS1-DENV2 differed
108 significantly between the two groups, with higher levels in the symptomatic group (Fig. 1D),
109 further supporting the role of pre-existing anti-NS1 IgA1 as a marker of disease risk. Next, to
110 corroborate the discriminative potential of IgA binding suggested by the ED_{50} analysis, we
111 assessed avidity by measuring antibody binding in the presence of urea as a chaotropic agent using
112 our multiplexed bead-based assay and compared pre-infection samples of those who subsequently
113 developed DF vs DHF/DSS[13]. Although individual antigen comparison did not reveal significant
114 differences between clinical groups (Extended Data Fig. 2A), a multivariate supervised approach
115 to assess the predictive value of IgA and IgG avidity for DHF/DSS showed that IgA avidity alone
116 predicted DHF/DSS with an accuracy of 92% (95% CI: 62%–99%, p = 0.014; fig. S2B, while IgG
117 avidity neither predicted outcome nor enhanced the model's performance (Extended Data Fig. 2B).

118 These findings establish pre-existing high-avidity IgA antibodies induced after a primary
119 ZIKV infection as key discriminative features associated with the development of DHF/DSS
120 during a subsequent DENV2 infection.

121

122 **Pre-existing anti-NS1 IgA antibodies drive neutrophil effector functions *ex vivo* in children**
123 **who developed DHF/DSS**

124 Although IgA antibodies have been mainly studied in the context of mucosal immunity, they
125 constitute the second most abundant immunoglobulin isotype in human serum, following
126 IgG1[14,15]. Neutrophils are the primary and most abundant effectors of IgA antibodies[16]. Notably,
127 IgA-mediated neutrophil activation is thought to contribute to the pathogenesis of IgA-mediated
128 immune diseases through formation of IgA-immune complexes[17]. Several IgA-mediated immune
129 diseases share clinical features with DHF/DSS, such as thrombocytopenia, arthralgia, petechiae
130 and kidney involvement[18]. Considering this, we investigated whether pre-existing IgA antibodies
131 could enhance neutrophil effector functions and be associated with the development of severe
132 dengue disease.

133 To evaluate the functional capacity of pre-infection antibodies elicited by prior ZIKV infection to
134 activate neutrophils upon engagement with antigens from the incoming DENV2 serotype (NS1
135 and E), we evaluated antibody-dependent neutrophil effector functions in *ex vivo* functional assays.
136 Considering that phagocytosis and NETosis are key neutrophil effector functions[19], we
137 implemented *ex vivo* functional assays to measure antibody-dependent neutrophil phagocytosis
138 (ADNP) and NETosis as a readout of antibody-dependent neutrophil activation. For ADNP, beads
139 were coupled with either E or NS1 from the incoming serotype (DENV2) at comparable antigen
140 densities (Extended Data Fig. 3A). The beads were opsonized with the pre-infection plasma of the
141 participants, and flow cytometry was used to assess neutrophil phagocytosis of the beads[20]. Our
142 results revealed that children who subsequently developed thrombocytopenia exhibited
143 significantly higher ADNP against NS1 compared to those who did not (Extended Data Fig. 3B).
144 In fact, ADNP against NS1 consistently exceeded ADNP against E across different clinical
145 endpoints of disease severity (Extended Data Fig. 3B). This observation prompted a comparison
146 of ADNP responses to NS1 vs. E among participants who developed DF or DHF/DSS and among
147 participants who developed features of severe disease such as thrombocytopenia, plasma leakage,
148 or hemorrhage. We found that the plasma from children who developed DHF/DSS or displayed
149 hallmarks of severe disease like plasma leakage or thrombocytopenia consistently induced higher
150 ADNP against NS1 than to E (Fig. 2A). Moreover, ADNP to NS1 was correlated with peak
151 hematocrit during the subsequent DENV2 infection, and this marker of plasma leakage was
152 strongly correlated with lower platelet count (Extended Data Fig. 3C). Further, IgA avidity to NS1,
153 but not IgG avidity, was positively correlated with ADNP to NS1 (Extended Data Fig. 3C).
154 Considering these observations and given that IgA antibodies against DENV2 NS1 showed the
155 highest adjusted coefficient in our multivariate model of antibody binding and were significantly
156 different across the spectrum of DENV infection (Fig 1B, D and Extended Data Fig. 1A), we
157 sought to determine whether the antibody-dependent neutrophil effector functions induced by pre-
158 existing antibodies were specifically driven by IgA and directed to NS1. To do this, we employed
159 a complementary experimental approach. Due to the technical challenges of purifying IgA from
160 small plasma volumes, we compared the ability of IgA-depleted and mock-depleted plasma to
161 induce NETosis in an *ex-vivo* functional assay[21]. In this assay, wells coated with either E or NS1
162 were incubated with IgA-depleted or mock-depleted pre-infection plasma, and the induction of
163 neutrophil extracellular traps (NETs) was quantified using a fluorescence-based assay.
164 Importantly, in the absence of antibodies, E and NS1 induced minimal NET formation (Extended

165 Data Fig. 4). Nevertheless, NS1 induced robust NETosis in the presence of mock-depleted serum
166 (Fig 2B). Upon IgA depletion, responses to E were heterogeneous with no difference between DF
167 and DHF/DSS, with some participants showing increased and others decreased neutrophil
168 activation (Fig. 2B, Supplemental Videos 1 and 2). However, the response to NS1 was consistently
169 reduced by IgA depletion in those who progressed to DHF/DSS (Fig. 2C, Supplemental Videos 3
170 and 4). All together, these results demonstrate that pre-existing antibodies, particularly IgA
171 targeting NS1, play a critical role in driving neutrophil effector functions, as evidenced by ADNP
172 and NETosis in *ex vivo* functional assays.

173

174 **Post-ZIKV severe DENV infections are characterized by enhanced neutrophil activation in**
175 **acute-phase plasma correlating with IgA binding to NS1**

176 Consequently, we evaluated neutrophil involvement during the subsequent acute DENV2 infection
177 in participants who progressed to DHF/DSS vs. DF. To do this, we assessed plasma samples
178 obtained during the acute DENV2 infection of the same 24 participants (DF=14, DHF/DSS=10)
179 from the PDCS. Initially, we evaluated circulating neutrophil levels during acute infection. On day
180 three post-fever onset, just before the emergence of severe disease, children who progressed to
181 DHF/DSS exhibited significantly higher relative neutrophil counts compared to those who
182 developed DF (Fig. 3, A and B).

183 Next, we examined neutrophil degranulation, a key neutrophil effector function measurable
184 in plasma. We analyzed levels of components of primary granules (myeloperoxidase [MPO],
185 neutrophil elastase [NE]), secondary granules (lactoferrin [LF]), and tertiary granules (matrix
186 metalloproteinase 9 [MMP-9]) in serum collected on days 1-3 post-fever onset (Table S1).
187 Importantly, MPO levels were significantly elevated in children with DHF/DSS, and primary
188 granule components (MPO and NE) were associated with heightened risk of developing severe
189 clinical manifestations, including mucosal bleeding, vascular leakage, and increased risk of ICU
190 admission (Fig. 3, C and D).

191 Thereafter, we evaluated whether this enhanced neutrophil degranulation was correlated
192 with antibody binding. In agreement with our experimental observation and statistical prediction
193 in pre-infection samples, IgA binding to NS1 positively correlated with levels of MPO, while IgG
194 antibodies correlated negatively with levels of MMP-9 (Fig. 3E). Importantly, binding of anti-NS1

195 IgA positively correlated with higher hematocrit (Fig 3E). This highlights a distinct association
196 between IgA antibodies targeting NS1, heightened neutrophil activation, and vascular leakage
197 early in the evolution to severe disease.

198 In this study, analysis of DENV2 viral load during acute infection revealed no significant
199 differences between clinical groups at the time of assessment (early post-fever onset; Fig. 3C), a
200 finding also observed in post-ZIKV DENV infections in a different population in Brazil[6].

201 These findings corroborate our experimental observations in pre-infection samples and *ex*
202 *vivo* functional assays and demonstrate that severe post-ZIKV DENV2 infections are characterized
203 by increased neutrophil activation that correlates with IgA antibodies in plasma binding to NS1.
204 Furthermore, these results highlight plasma IgA antibodies directed against NS1 as key drivers of
205 enhanced neutrophil activation during acute DENV2 infection.

206

207 **Enhanced neutrophil activation precedes the development of vascular leakage and**
208 **progression to DHF/DSS**

209 To validate our findings, we investigated neutrophil involvement in the Pediatric Dengue Hospital-
210 based Study (PDHS), an independent study conducted in Managua, Nicaragua. This study enrolls
211 participants under 15 years of age presenting with acute febrile illness suspected of dengue; DENV
212 infections are laboratory-confirmed and serotyped by RT-PCR[22]. We screened children in the
213 PDHS with DENV2 infections during the 2018–2020 epidemic to identify those with prior ZIKV
214 exposure using our serotyping approach[4,12].

215 A total of 111 dengue cases with past ZIKV infections were identified (DF=67,
216 DHF/DSS=44). Consistent with the PDCS observations, children who developed DHF/DSS
217 exhibited significantly higher neutrophil counts compared to those with DF prior to progression to
218 DHF/DSS (Fig. 4A and Extended Data Fig. 5A). We further explored neutrophil activation in a
219 subset of samples (18 DHF/DSS and 36 DF cases) collected early after fever onset (≤3 days post
220 fever onset), matched for age and sex. As in prior analyses, significantly elevated markers of
221 neutrophil degranulation, particularly MPO and NE components of primary granules, were
222 observed in individuals who progressed to DHF/DSS (Fig. 4B). Importantly, neutrophil
223 degranulation markers (MPO) were associated with anti-NS1 IgA binding, but not with IgA
224 binding to E nor with IgG antibodies to NS1 or E (Fig. 4C and D). In addition, while anti-NS1 IgA

levels positively correlated with hematocrit in the PDCS (Fig 3E), in the PDHS anti-E IgG antibodies were associated with lower hematocrit, a marker of lesser vascular leakage (Fig. 4C and D). Finally, we investigated whether neutrophil degranulation preceded the development of vascular leakage, a defining feature of DHF/DSS. To address this, we used gallbladder wall thickness as a quantitative marker of vascular leakage[23–25]. Gallbladder wall edema, a result of vascular leakage, is observed as DENV infection progresses to severe disease (Fig. 5A). This ultrasonographic metric provides a robust, continuous measure that is unaffected by treatment interventions and is widely and consistently employed in our setting for clinical triage and follow-up[23]. We found that the maximum gallbladder wall thickness – typically reached on day 4 post-fever onset or later (Fig. 5A) – was positively correlated with levels of the primary granule component NE measured on day 3 or earlier in both PDCS and PDHS participants (Fig. 5B and C). These findings reveal that neutrophil activation precedes vascular leakage, implicating a role in the pathogenesis of severe dengue disease.

Discussion

The introduction of ZIKV into endemic regions of Latin America resulted in the widespread co-circulation of ZIKV and the closely related flaviviruses, DENV1-4. ZIKV continues to circulate alongside the four DENV serotypes at low levels in Asia and sporadically in Latin America[26]. Like sequential DENV infections with different serotypes, prior ZIKV immunity increases the risk of subsequent severe dengue disease [4,5]. However, we and others found that post-ZIKV DENV infections that progress to severe disease do not exhibit the elevated viral load associated with antibody-enhanced DENV infections[6]. This suggests that alternative immune mechanisms may contribute to the heightened risk of severe disease in these cases. Therefore, we performed an agnostic serological analysis of potential biomarkers correlated with the risk of subsequent severe dengue disease. Surprisingly, plasma IgA antibodies were key discriminative features between clinical groups. Thus, we focused on plasma IgA, an often-overlooked antibody isotype in immune responses to infectious diseases. Our findings demonstrate that plasma IgA antibodies targeting NS1 drive neutrophil activation in severe post-ZIKV dengue disease. Importantly, we establish a temporal relationship between pre-existing anti-NS1 IgA antibodies and heightened neutrophil activation during the subsequent acute infection. In addition, we show that this increased

255 neutrophil activation not only precedes but also correlates with the development of vascular
256 leakage – a critical hallmark of severe dengue disease.

257 IgA antibodies in human serum are present at concentrations comparable to IgG3 and
258 IgG2[14,15]. Although extensively studied in mucosal immunity, the role of IgA antibodies in human
259 serum – whether protective or pathogenic – has been largely overlooked in infectious diseases.
260 This gap partly reflects limitations in mouse models, which naturally lack CD89 (Fc alpha
261 receptor), a critical receptor for IgA on human myeloid cells[27]. Of note, elevated IgA immune
262 complexes have been implicated in autoimmune diseases through neutrophil activation; these
263 diseases share clinical features with dengue, such as rash, petechiae, thrombocytopenia, and kidney
264 involvement[17,18,28]. In the context of infectious diseases, serum IgA antibodies can mediate virus
265 neutralization[29], and DENV IgA antibodies targeting structural components can block ADE and
266 neutralize the virion[30]. In contrast, our study demonstrates that IgA antibodies against NS1, a non-
267 structural protein that is secreted during flavivirus infection, induce neutrophil activation in
268 DHF/DSS preceding vascular leakage. While previous studies have reported DENV-associated
269 IgA nephropathy and elevated titers of IgA in children with DHF/DSS[31,32], the absence of a
270 temporal relationship between IgA responses and disease progression has hindered understanding
271 of its role in DENV pathogenesis. By analyzing samples collected after primary ZIKV infection
272 and prior to subsequent DENV2 infection, we establish a temporal link between pre-existing
273 ZIKV-induced IgA antibodies targeting DENV NS1 and heightened neutrophil activation,
274 development of disease, and progression to DHF/DSS.

275 Importantly, heightened neutrophil activation has consistently been associated with severe
276 dengue disease in humans[33–35]. Indeed, genes associated with increased neutrophil functions have
277 been proposed as prognostic markers of severe dengue[36,37]. Nevertheless, the link between
278 neutrophil activation and pre-existing antibodies, a major risk factor for DHF/DSS, has remained
279 elusive. Interestingly, DENV induces the production of immature neutrophils[38], which
280 predominantly synthesize primary granules containing MPO and NE – degranulation markers
281 associated with DHF/DSS. In parallel, serum IgA, to a greater extent than IgG, has been shown to
282 enhance neutrophil effector functions during viral infections[39,40]. Based on these observations and
283 our results, we hypothesize that IgA/NS1 immune complexes drive heightened activation of
284 immature neutrophils during infection, contributing to vascular dysfunction and organ damage.
285 The pathogenic role of neutrophil activation has been well-documented in other infectious

286 diseases, such as malaria and leishmaniasis[41,42]. Although the current understanding of DHF/DSS
287 immunopathogenesis is centered on the role of IgG antibodies targeting structural components of
288 the virion in the context of ADE[9,10], we believe that enhanced neutrophil activation due to cross-
289 reactive anti-NS1 IgA antibodies may contribute to disease pathogenesis in sequential DENV
290 infections.

291 Nonetheless, our study has several limitations. First, our work was not intended to define
292 the entire pathogenic cascade leading to severe disease, but rather to illustrate a plausible
293 immunological pathway linking pre-existing IgA immunity to downstream neutrophil responses
294 specific to the incoming serotype. Existing murine DENV disease models lack expression of the
295 Fc alpha receptor (CD89) and exhibit IgA immunobiology distinct from humans[27]. This limited
296 our ability to validate IgA-mediated neutrophil activation as a direct cause of vascular leakage and
297 define specific neutrophil effector functions leading to severe disease. Instead, we investigated the
298 functional capacity of human IgA antibodies elicited by prior ZIKV infection to activate
299 neutrophils upon binding to NS1 or E antigens from the incoming DENV serotype. We conducted
300 *ex vivo* functional assays using primary cells from healthy human donors, which demonstrated a
301 strong association between IgA antibodies targeting NS1, neutrophil activation, and severe
302 disease. We showed that IgA depletion in the presence of NS1 but not E significantly reduced
303 neutrophil effector functions, underscoring the specificity of this response. Then, we validated this
304 experimental observation in two independent human studies during acute DENV2 infection.

305 However, our findings should be interpreted in light of the limitations of plasma
306 biomarkers of neutrophil effector functions. We measured neutrophil degranulation and circulating
307 NETs *in vivo* during the early phase of acute DENV infection. Nevertheless, circulating NET
308 remnants may not reliably reflect the extent of NET formation in tissue sites where pathology
309 occurs. Additionally, the timing of sample collection—restricted to the early febrile phase—may
310 well not be optimal for capturing differences in NETosis. Unfortunately, matched samples from
311 later timepoints in both the PDHS and PDCS, when NETosis may be more pronounced, are not
312 available. Although we could not delineate the entire pathogenic cascade leading to severe disease,
313 we demonstrate a plausible immunological mechanism linking pre-existing serum IgA immunity
314 targeting NS1 of the incoming serotype to downstream neutrophil responses. This temporal
315 connection represents a key strength of our study.

316 In addition, our findings suggest distinct roles for IgA antibodies targeting NS1 versus
317 structural components such as E. The observed discrepancy between the capacity of anti-NS1 and
318 anti-E IgA antibodies to trigger neutrophil activation raises important mechanistic questions that
319 warrant further investigation. While both antigens were used under similar coupling densities, our
320 findings suggest that the differences in neutrophil activation are not due to intrinsic properties of
321 the antigens themselves. This is supported by the observation that neither NS1 nor E alone
322 triggered NET formation. A more plausible explanation lies in the properties of the immune
323 complexes formed with polyclonal sera. Variations in antibody abundance, avidity, stoichiometry,
324 and/or epitope specificity between anti-NS1 and anti-E antibodies could influence the
325 configuration and density of Fc receptor engagement on neutrophils. These factors, in turn, may
326 modulate the strength and nature of downstream signaling required for neutrophil activation. While
327 our current data are consistent with this hypothesis, a detailed mechanistic dissection of immune
328 complex architecture, Fc receptor cross-linking, and signaling dynamics remains beyond the scope
329 of this study and will require future molecular and biophysical analyses. Future studies are needed
330 to elucidate these mechanisms and their broader consequences in the immunopathogenesis of viral
331 infections.

332 Our study has several significant implications, as we explored the pathogenic role of
333 plasma IgA antibodies, a frequently overlooked antibody isotype in immune responses. Our
334 findings highlight the critical interplay between antigenic target and antibody isotype in disease
335 and protection. While IgA antibodies targeting E can counteract ADE from IgG against the
336 structural components of the virion[30] and IgG anti-NS1 antibodies confer protection against the
337 virulent properties of NS1[43,44], our results show that anti-NS1 IgA antibodies are implicated in
338 severe disease. Furthermore, while we do not exclude IgG-mediated ADE, our observations
339 support the presence of an alternative pathogenic pathway mediated by IgA antibodies and
340 neutrophil activation in DENV infection. This highlights an interesting therapeutic avenue, since
341 neutrophil functions can be targeted by approved and emerging drugs[45]. Moreover, our findings
342 underscore the importance of evaluating isotype- and antigen-specific antibody profiling of
343 humoral immune responses induced by DENV and ZIKV vaccines. While further validation across
344 diverse geographic and demographic settings is needed, our results suggest that binding and avidity
345 of anti-NS1 IgA antibodies may serve as predictive markers of subsequent severe dengue disease.
346 Similarly, the assessment of neutrophil degranulation early during DENV infection could provide
347 a valuable triaging tool for identifying patients at risk of DHF/DSS.

348 Finally, our findings enrich the current understanding of the role of pre-existing immunity
349 in the immunopathogenesis of severe dengue disease. We leveraged a key strength of the PDCS
350 —namely, its unique ability to enable immune profiling in both pre-infection and acute-phase
351 plasma samples in the same participants — and validated our findings in acute-phase samples from
352 the PDHS as an orthogonal study. Using binding assays, *ex-vivo* functional assays, and validation
353 of our observations in paired pre-infection and acute samples as well as an orthogonal study, we
354 show that IgA antibodies drive neutrophil activation that correlates with increased risk of severe
355 disease and precedes vascular leakage. We underscore the importance of antibody isotypes beyond
356 IgG, such as IgA, and their antigenic targets (NS1 vs. E), with implications for establishing
357 biomarkers of risk, refining therapeutic strategies, and informing vaccine development. Further
358 research into the precise mechanisms of IgA-mediated neutrophil activation is essential to fully
359 unravel the pathways driving severe disease in the context of flaviviral and other infectious
360 diseases.

361

362 **Materials and Methods**

363 Ethics statement

364 The Pediatric Dengue Cohort Study was reviewed and approved by the institutional review boards
365 of the University of California, Berkeley (protocol 2010-09-2245), the University of Michigan
366 (HUM00091606), and the Nicaraguan Ministry of Health (NIC-MINSA/CNDR CIRE-09/03/07-
367 008). The Pediatric Dengue Hospital-based Study was reviewed and approved by the institutional
368 review boards of the University of California, Berkeley (2010-06-1649) and the Nicaraguan
369 Ministry of Health (NIC-MINSA/CNDR CIRE-01/10/06-13). Parents or legal guardians of all
370 subjects provide written informed consent, and subjects ≥6 years old provide assent.

371

372 Study design

373 The primary objective of this study was to identify antibody biomarkers associated with the risk
374 of developing severe dengue after a primary ZIKV infection during a subsequent DENV2
375 infection. Serum samples were obtained from participants enrolled in the Pediatric Dengue Cohort
376 Study (PDCS), as described below. These participants had a documented primary ZIKV infection
377 in 2016 and then experienced a DENV2 infection in the 2019-2020 dengue season. During the

378 DENV2 infection, children developed either dengue fever (DF, n=14) or dengue hemorrhagic
379 fever/dengue shock syndrome (DHF/DSS, n=10). We evaluated serum samples collected after the
380 primary ZIKV infection and 4-10 months before the secondary DENV2 infection in order to
381 identify antibody biomarkers of risk, using our multiplexed bead-based approach[12], as described
382 below.

383 The primary endpoint was the clinical classification of DF versus DHF/DSS, based on the
384 WHO 1997 guidelines (see below). Secondary endpoints included the presence of plasma leakage,
385 hemorrhagic manifestations, and thrombocytopenia. We also used gallbladder wall thickness,
386 assessed by ultrasonography, as a surrogate of vascular leak[23].

387 Following the identification of humoral biomarkers correlated with clinical outcomes (i.e.,
388 IgA antibodies targeting the viral NS1 protein), we investigated their role in disease pathogenesis.
389 Given that neutrophils are the most abundant and primary effectors of IgA antibodies[16], we
390 performed *ex vivo* functional assays to evaluate antibody-dependent neutrophil effector functions
391 (see below). Additionally, we examined the involvement of neutrophils and their correlation with
392 antibody binding using paired acute-phase samples from the same participants of the PDCS during
393 the acute secondary DENV2 infection. Finally, the findings were further validated with an
394 independent dataset from the Pediatric Dengue Hospital Study (PDHS), evaluating participants
395 who experienced a DENV2 infection during 2018 to 2020 with a history of primary ZIKV
396 infection.

397

398 Description of studies

399 The **Pediatric Dengue Cohort Study (PDCS)** is an ongoing prospective cohort study initiated in
400 2004 and based at the Sócrates Flores Vivas Health Center (HCSFV), the primary health care
401 facility for District II of Managua, and part of the Municipal Health System of Managua. Located
402 adjacent to Lake Xoxitlan, District 2 encompasses neighborhoods spanning a spectrum of low to
403 middle socioeconomic status. The HCSFV serves ~62,000 residents across 18 neighborhoods
404 within District II[46]. The illiteracy rate in this area is approximately 7%, and over 90% of the
405 households have access to running water and a sewage system. All residents have access to
406 electricity. The PDCS tracks approximately 4,000 active participants yearly and has followed
407 ~9,800 children since its initiation. To preserve the original age distribution of the cohort,
408 approximately 250 two-year-old children, along with children aged 3-11 years as needed, are
409 enrolled annually. Adjustments to the age limit were implemented in 2018, 2019, and 2022,

410 extending the eligibility to 15, 16, and 17 years, respectively. Participants benefit from free, round-
411 the-clock medical care provided by study physicians at the HCSFV. In cases requiring
412 hospitalization, study staff facilitate patient transfer to the study hospital, the National Pediatric
413 Reference Hospital (Hospital Infantil Manuel de Jesús Rivera). Children presenting with fever and,
414 since July 2016, rash are screened for signs and symptoms of dengue, Zika, and chikungunya.
415 Symptomatic infections are captured through "enhanced" passive surveillance, complemented
416 with periodic home visits. For each suspected case, both acute (0-6 days post-symptom onset) and
417 convalescent samples (14-21 days) are collected to confirm infection. Approximately 97% of cases
418 present to the HCSFV within the first three days of illness, and convalescent samples are collected
419 from 94% of cases (Kuan et al 2009 AJE). Additionally, the study collects annual healthy blood
420 samples from all participants in March-April (previously in July before 2011), which enables the
421 detection of inapparent arboviral infections[11].

422 The **Pediatric Dengue Hospital-Based Study (PDHS)** is based at the Hospital Infantil
423 Manuel de Jesús Rivera (HIMJR), Managua, Nicaragua (2005-present)[22,47]. Children are invited
424 to participate if they: 1) present to the hospital 1-7 days post-onset of symptoms and 2) meet case
425 definitions for dengue, Zika, and/or chikungunya, which consists of either i) ≥1 signs or symptoms,
426 including headache, arthralgia, myalgia, retro-orbital pain, positive tourniquet test, petechiae, or
427 signs of bleeding; or ii) rash with ≥2 signs/symptoms including fever, conjunctivitis, arthralgia,
428 myalgia, or peri-articular edema[22]. Blood samples are collected at presentation (acute), daily for
429 days 1-3, and at convalescence (14-28 days). Infections are defined as for the cohort using RT-
430 PCR, virus isolation, and DENV, ZIKV, and CHIKV serological assays (detailed below). Clinical
431 information (>150 variables) and fluid intake/output is collected every 12 hours, and, after
432 systematic monitoring by a clinical supervisor, is digitized by double-data entry, with quality
433 control checks performed daily and weekly. A standardized questionnaire is used to record the
434 subject's demographic and epidemiologic characteristics. As part of a longitudinal arm of the
435 study, consenting participants return to provide healthy blood samples 3, 6, 12, and 18 months
436 post-illness.

437

438 Case definitions

439 **Primary ZIKV infection in the PDCS** was defined as DENV- and ZIKV-naïve participants who
440 presented with fever or rash after July 2016 and were clinically classified as either: A) meeting the

441 1997 and/or 2009 WHO criteria for dengue, or B) having an undifferentiated febrile illness.
442 Laboratory confirmation of ZIKV infection was performed as described below.

443 **Primary ZIKV infection in the PDHS** was defined as participants meeting criteria A or
444 B during 2018–2019 and showing evidence of a monotypic ZIKV antibody response early in
445 infection (<4 days post-fever onset), as defined in [4] or [12] (detailed below).

446 **Second DENV2 infection** was defined as children who met the criteria for primary ZIKV
447 infection and subsequently developed a DENV2 infection during 2019–2020 in the PDCS or 2018–
448 2020 in the PDHS. Children experiencing a second DENV2 infections were classified as DF or
449 DHF/DSS based on the criteria described below.

450

451 Laboratory confirmation of ZIKV and DENV infections in the PDCS

452 All cases meeting definitions A or B were evaluated for acute ZIKV or DENV infections, with
453 laboratory confirmation performed by: 1) real-time RT-PCR (rRT-PCR) and/or viral isolation from
454 acute serum (and/or urine for ZIKV); 2) seroconversion detected via ZIKV or DENV IgM capture
455 (MAC)-ELISA; and/or 3) seroconversion or a ≥4-fold increase in DENV- or ZIKV-specific
456 iELISA titers in paired acute and convalescent sera[11,48]. The infecting virus (DENV or ZIKV) was
457 determined based on rRT-PCR results[49,50]. RT-PCR-negative cases were classified as 1) ZIKV if
458 seroconversion or a ≥4-fold rise in ZIKV-specific titers was detected, or, for arbovirus cases in
459 2016–2017, if identified as ZIKV-positive by a computational classification algorithm[51], or 2)
460 Flavivirus cases if seroconversion or a ≥4-fold increase was observed in both DENV and ZIKV
461 assays. Flavivirus cases and cases with confirmed RT-PCR or viral isolation evidence of co-
462 infection with DENV and ZIKV were excluded from the analyses. All secondary DENV2
463 infections were confirmed by rRT-PCR[49].

464

465 Inclusion and exclusion criteria

466 All participants from the PDCS who had a documented primary ZIKV infection in 2016 followed
467 by a second DENV2 infection during 2019-2020, with the second infection classified as DHF/DSS
468 according to WHO 1997 criteria, were included (n=10). Additionally, 14 participants with a similar
469 infection history who developed DF, matched by sex and age, were selected as a comparison group
470 using convenience sampling, as well as 18 participants with the same infections history who
471 developed a second inapparent DENV2 infection. The entire sample set (DF vs. DHF/DSS) was

472 used for analysis of neutrophil counts during infection, excluding 7 participants with missing
473 neutrophil counts on day 3 post-fever onset (Fig. 3B).
474
475 In the PDHS, a total of 362 confirmed DENV2 infections were documented between 2018
476 and 2020. Among these, 261 cases were classified as DF and 65 as DHF/DSS. All 65 DHF/DSS
477 and a convenience sample of 103 DF cases were serotyped to identify second DENV2 infections
478 after a primary ZIKV, using the methods described in [4] and [12] (detailed below). A total of 111
479 participants with past ZIKV infections were identified (DF=67, DHF/DSS=44). This entire sample
480 set was used for analysis of neutrophil counts during infection, excluding 2 participants with
481 missing neutrophil counts (Fig. 4A).
482 For our orthogonal confirmation of neutrophil involvement during acute DENV2 infection,
483 we determined the sample size using Cohen's *d* effect size and power analysis[52]. Based on our
484 observations in the PDCS, the estimated effect size was d = -0.9128 (95% CI: -1.8139, -0.0117),
485 corresponding to a large effect size. To achieve a statistical power of 80% (β = 0.20) at a
486 significance level of 0.05 (α = 0.05) for a one-tailed two-sample *t*-test (assuming normal data
487 distribution), a minimum of 16 participants per group (DF vs. DHF/DSS) was required.
488 Accordingly, to analyze the temporal relationship between neutrophil functions and progression
489 to severe disease, we selected a subsample of 18 DHF/DSS cases with serum samples collected on
490 day 3 post-fever onset or earlier. These cases were matched by sex and age with 36 DF cases whose
491 serum samples were also collected during acute infection (day 3 post-fever onset or earlier). This
492 dataset was used to compare neutrophil degranulation among clinical groups and to evaluate the
493 correlation of neutrophil degranulation with the maximum documented thickness of the
494 gallbladder wall. Participant characteristics are summarized in **Table S1**. The plot in Fig. 5A
495 included 7 DF and 10 DHF/DSS with gallbladder thickness information from the PDCS, and 66
496 participants with DF and 43 participants with DHF/DSS from the PDHS.
497
498 Definition of severe dengue disease

499 Severe disease in our study was defined as a composite outcome of children meeting the WHO
500 1997 criteria for Dengue Hemorrhagic Fever or Dengue Shock Syndrome. **Dengue Hemorrhagic**
501 **Fever** was defined as experiencing at least one of each of the following criteria: fever plus 1)
502 hemorrhagic manifestations defined as the presence of at least one of the following manifestations:
503 i) positive tourniquet test, ii) ecchymosis, petechia, hematoma, purpura, iii) bleeding at injection

site, hypermenorrhea or vaginal bleeding, subconjunctival hemorrhage, hematuria, hemoptysis, bleeding gums or nose, iv) hematemesis or melena; 2) thrombocytopenia defined as platelet count ≤100,000 platelets per mm^3; 3) evidence of plasma leakage as a result of increased vascular permeability defined as i) ≥20% hemoconcentration, ii) age- and sex-specific elevated hematocrit, iii) pleural effusion, iv) ascites, v) hypoproteinemia or hypoalbuminemia, or vi) edema. **Dengue Shock Syndrome** (1997 WHO criteria) was defined as cases meeting criteria for DHF and at least one of each of the following criteria: 1) i) age-specific hypotension or ii) narrow pulse pressure <20 mmHg), and 2) i) cold, clammy skin and restlessness or ii) rapid and weak pulse. Symptomatic participants infected with DENV2 who did not meet the criteria for severe disease were categorized as having **Dengue Fever (DF)**. Additionally, secondary endpoints for the study included the presence of hemorrhagic manifestations, thrombocytopenia, or plasma leakage, as defined by the established criteria.

Viral load quantification

Viral RNA was extracted from virus particles using the QIAmp kit (QIAGEN). The PCR standard curve used for the quantification of DENV genome copies was obtained with an amplicon containing a synthetic cDNA encompassing a fragment of the NS5 region (nucleotides 9937–10113) from DENV2 strain DENV2 (8971.12a1SPD2; Genbank; MZ008454.1). Absolute quantitation of viral RNA was determined by real-time quantitative RT-PCR (RT-qPCR) using the following primer and probe sequences: DENV2 forward (ACAAGTCGAACAACCTGGTCCAT), reverse (GCCGCACCATTGGTCTTCTC) and probe (FAM- CCAGTGGAATCATGGGAAGAAGTCC CA-TAMRA. The Verso 1-step RT-qPCR kit (Thermo Fisher Scientific) was used following the manufacturer's instructions. Standard curves were prepared using seven 10-fold dilutions of a DENV2 (8971.12a1SPD2; Genbank; MZ008454.1) synthetic fragment. Reaction mixtures were run in a QuantStudio 3 thermocycler (Applied Biosystems), and the quantity values were used for analyses[53,54].

EDIII serotyping in the PDHS

The EDIII serotyping of early acute serum samples (<4 days post-fever onset) from the PDHS was conducted as described in[12]. Briefly, recombinant EDIII proteins for DENV1-4 and ZIKV (courtesy of Dr. Lakshmanane Premkumar, University of North Carolina [UNC], Chapel Hill)

535 were site-specifically biotinylated and conjugated to avidin-coated MagPlex Luminex beads.
536 These antigen-coupled microspheres were combined and incubated in 384-well plates with
537 appropriately diluted plasma (four 4-fold dilutions starting at 1:50). Each well contained 500
538 microspheres per antigen and was incubated for 90 minutes at 37°C, shaking at 1200 rpm.
539 Following incubation, the plates were washed with phosphate-buffered saline (PBS) containing
540 0.1% bovine serum albumin (BSA) and 0.02% Tween 20 using an automatic magnetic washer
541 (Tecan Hydrospeed). Antigen-specific IgG binding was detected with phycoerythrin (PE)-
542 conjugated mouse anti-human total IgG (SouthernBiotech #9040-09). Median fluorescence
543 intensity (MFI) was measured using an iQue3 (Intellicyt) instrument, set to acquire at least 50
544 beads per bead region. DENV-naïve human serum was included in triplicate on each plate as a
545 negative control. MFI values for EDIII-DENV1, EDIII-DENV2, EDIII-DENV3, EDIII-DENV4,
546 and EDIII-ZIKV were transformed as the relative proportion of the highest MFI observed at a
547 serum dilution of 1:800. Then, a heatmap with hierarchical clustering using Wald's method was
548 generated, identifying five distinct clusters corresponding to DENV1-4 and ZIKV. The prior
549 infecting virus (DENV1-4 or ZIKV) was assigned based on the antigen with the highest MFI value
550 and the grouping within the cluster analysis. Finally, an empirical cutoff value was applied to
551 distinguish monotypic EDIII ZIKV responses[12]. Specifically, for a sample to be classified as past
552 primary ZIKV infection, the second highest MFI signal should be lower than 20% of the maximum
553 ZIKV EDIII signal. Prior ZIKV infections were successfully detected in acute-phase sera from the
554 PDHS using a similar EDIII-based method in[4].
555
556 Multiplex bead-based antibody binding and avidity assay
557 Recombinant E and NS1 proteins from DENV1-4 and ZIKV were commercially acquired from
558 Native Antigen Co. (United Kingdom). Recombinant EDIII of DENV1-4 and ZIKV were site-
559 specifically biotinylated and provided as a gift by Dr. Premkumar (UNC, Chapel Hill). Antibody
560 subclass and isotype binding in pre-infection samples was determined using a multiplex bead-
561 based assay, as previously described[12]. Briefly, E and NS1 from DENV1-4 and ZIKV were
562 randomly biotinylated according to the manufacturer's instructions (EZ-Link™ Sulfo-NHS-LC-
563 LC-Biotin, No-Weigh™ Format; Thermo Fisher Scientific) and desalted using Zeba Spin Columns
564 (Thermo Fisher Scientific). The randomly biotinylated E and NS1 and the site-specifically
565 biotinylated EDIII from DENV1-4 and ZIKV were conjugated to avidin-coated MagPlex Luminex
566 beads. Immune complexes were formed in 384-well plates by mixing the appropriately diluted

567 plasma (six 4-fold dilutions) with antigen-coupled microspheres for 90 minutes at 37°C, shaking
568 at 1200 rpm. After incubation, plates were washed using an automatic magnetic washer (Tecan
569 Hydrospeed) with PBS containing 0.1% BSA and 0.02% Tween 20. For avidity testing, samples
570 were washed for ten minutes with urea 7M or with PBS. Afterward, plates were washed again with
571 PBS containing 0.1% BSA and 0.02% Tween 20. Finally, antigen-specific subclass/isotype
572 binding was detected using PE-coupled mouse anti-human detection antibodies against IgA
573 (SouthernBiotech #2050-09), IgM (SouthernBiotech #9020-09), total IgG (SouthernBiotech
574 #9040-09), IgG1 (Southern-Biotech #9052-09), IgG2 (SouthernBiotech #9060-09), IgG3
575 (Southern-Biotech #9210-09), and IgG4 (SouthernBiotech #9200-09). Fluorescence was acquired
576 using an iQue3 (Intellicyt) machine (Sartorius), as described above. Antigen-specific antibody
577 subclass/isotype binding was extracted as median fluorescence intensity (MFI). Then, a netMFI
578 was calculated by subtracting the background binding of a DENV-naïve sample from each test
579 sample. Then, we fitted a dose-response curve using the netMFI across six 4-fold serial dilutions
580 of plasma to estimate the effective dilution 50 (ED_{50}) of the binding for each tested antigen,
581 antibody subclass/isotype, and participant using the *drda* package v2.0.3. For calculating the
582 Avidity Index (AI), the area under the curve (AUC) of the binding after washing with Urea or PBS
583 was estimated, and then compared using the formula AI = AUC[Urea]/AUC[PBS]. Antigen-
584 specific binding in acute phase samples was performed with E, NS1, and E dimer from DENV2.
585 The recombinant stabilized envelope E dimer of DENV2 was purchased from the UNC Protein
586 Expression and Purification Core[55]. Binding during the acute phase was analyzed as the AUC of
587 the binding curve fitted using a dose-response model[54].
588
589 <u>IgA depletion from serum</u>

590 IgA antibodies were depleted from serum using the CaptureSelect™ IgA-XL Affinity Matrix resin
591 (Thermo Scientific™) with a spin column method. Briefly, disposable Mobicol spin columns were
592 prepared by loading either the CaptureSelect™ IgA affinity resin for depletion or empty agarose
593 beads for mock depletion. The resins were equilibrated with PBS (pH 7.4) prior to sample
594 application to ensure optimal binding conditions.
595 For depletion or mock-depletion, human serum diluted 1:50 was applied to the column
596 containing the IgA-specific resin or empty resin. The column was incubated on a rotating wheel at
597 room temperature for 30 minutes to allow antibody binding. After incubation, the column was
598 centrifuged at 700 × g for 1 minute to collect the flow-through, which contained the IgA-depleted

599 or mock depleted serum. Antibody binding, IgA depletion, and mock-depletion was confirmed in
600 validation samples using the previously described antibody binding and isotype characterization
601 multiplex bead-based protocol. Depleted and mock-depleted samples were stored at -80°C until
602 further analysis.
603
604 Antibody-dependent neutrophil phagocytosis and NETosis

605 Functional neutrophil *ex vivo* assays were conducted using neutrophils from three independent
606 healthy human donors: two donors for antibody-dependent neutrophil phagocytosis (ADNP) and
607 one donor for NETosis. Neutrophils were stimulated with immune complexes formed from pre-
608 infection serum antibodies and the antigen of interest, as detailed below.
609 ADNP was performed as previously described[20]. Antigens (NS1-DENV2 or E-DENV2,
610 Native Antigen Co.) were biotinylated and coupled to yellow-green neutravidin beads (Invitrogen).
611 Immune complexes were formed by mixing coupled beads with plasma. Plasma was diluted 1:25
612 in assay buffer (PBS with 1% BSA and 0.05% Tween-20), based on prior titration experiments
613 optimizing the dynamic range of the assay while minimizing background signal, and incubated
614 with beads for immunocomplex formation for 2 hours at 37°C. White blood cells were isolated
615 from fresh peripheral blood from healthy donors by performing ammonium-chloride-potassium
616 lysis of red blood cells. The isolated white blood cells were then added to 96-well plates at a
617 concentration of 2.5×10^5 cells/ml, and neutrophils were identified using anti-CD66b PacBlue
618 (BioLegend, 305112). Fluorescence was acquired using an iQue3 machine. A phagocytic score
619 was calculated using the following formula: (percentage of bead-positive cells) x (geometric mean
620 of MFI of bead-positive cells)/10,000. The results were summarized as the mean of the two
621 independent experiments for each serum sample, and the value was normalized using the min-max
622 approach. For this normalization, each value was rescaled using the formula: Normalized value =
623 $(x-min)/(max-min)$, where x is the individual phagoscore value, and min and max are the minimum
624 and maximum values observed across all samples in the assay per antigen.
625 For NETosis, neutrophils were isolated from whole blood collected in EDTA tubes from
626 one healthy donor under protocol #2303138796A001 at the Ponce Health Sciences University and
627 Ponce Research Institute in Puerto Rico, using the EasySep Direct Human Neutrophil Isolation
628 Kit (Stemcell Technologies, Catalog #19666). Cells were resuspended in Gibco Opti-MEM Serum
629 Reduced Media (ThermoFisher, Catalog #31985070). To generate fixed immune complexes (ICs),
630 NS1 or E protein (2 μg/mL) was plated in a 96-well plate and incubated overnight at 4°C with

631 medium (negative control), Phorbol myristate acetate (PMA) as positive control, and mock-
632 depleted or IgA-depleted samples. After protein coating, wells were washed three times with 1X
633 PBS and then incubated with a 1:25 dilution of serum in 1X PBS (100 µL per well) overnight at
634 4°C. Wells were then washed three times with sterile 1X PBS containing 0.05% Tween 20 and
635 then one time with 1X PBS before adding neutrophils. Neutrophils (30,000 cells/well) were added
636 to each well in 100 µL of Gibco Opti-MEM containing 250 nM Cytotox Green (Essen BioScience,
637 Catalog #4633). Plates were placed in an Incucyte SX5 instrument (Sartorius AG, Göttingen,
638 Germany) for live-cell imaging. Phase-contrast and green fluorescence images were captured at
639 20X magnification, with an exposure time of 300 milliseconds for green fluorescence. Images
640 were acquired every 30 minutes for 6 hours, with two images per well from distinct regions. The
641 Incucyte software was trained to differentiate between normal cells and those undergoing DNA
642 release using representative images from non-stimulated and stimulated cells. For analysis, the
643 software applied surface-fit background correction with a fluorescence threshold of 2.0 Green
644 Calibrated Units (GCU), edge sensitivity of -25, and a minimum mean intensity of 100. Phase-
645 contrast analysis used artificial intelligence (AI) confluence detection. The software automatically
646 analyzed the images and calculated the total integrated green intensity (GCU x μm^2/ image) per
647 well to quantify DNA release associated with NETosis. Paired IgA-depleted and mock-depleted
648 samples were compared for each antigen to calculate the percentage of signal loss due to IgA
649 depletion. To ensure comparability across samples, the percentage of signal loss was determined
650 at the timepoint of the slope of the positive control (after one hour of stimuli) using the formula:
651 Percentage change in signal = (IgA-depleted - IgA mock-depleted)/IgA mock-depleted * 100. The
652 results were expressed as percentages, ranging from -100% to +100%.
653
654 Quantification of markers of neutrophil degranulation

655 Neutrophil degranulation and NETosis were assessed in serum immediately after thawing, using
656 commercially available kits following the manufacturers' protocols. Myeloperoxidase (MPO) and
657 Matrix Metalloproteinase-9 (MMP9) concentrations in plasma were quantified using DuoSet™
658 ELISA kits (R&D Systems, DY3174 and DY911, respectively). Briefly, 96-well plates were
659 coated with specific capture antibodies diluted in PBS (pH 7.2–7.4) and incubated overnight at
660 room temperature. Plates were blocked with 1% BSA in PBS for 1 hour at room temperature.
661 Samples and standards, diluted in PBS with 1% BSA (with 2% normal goat serum for MMP9),
662 were added (100 µL/well) and incubated for 2 hours at room temperature. Detection antibodies

663 conjugated to biotin were applied, followed by a 20-minute incubation with streptavidin-horse
664 radish peroxidase (HRP). Signal development was achieved using tetramethylbenzidine (TMB),
665 and the reaction was stopped with 2N sulfuric acid. Optical density (OD) was measured at 450 nm
666 with background correction at 570 nm. Standard curves were generated using serial dilutions of
667 recombinant MPO and MMP9, and sample concentrations were interpolated using linear
668 regression.

669 Human neutrophil elastase (NE) concentrations in plasma were quantified using the Hycult
670 Biotech commercial kit (HK319). Plasma samples were diluted and added to microtiter wells pre-
671 coated with a human elastase-specific capture antibody. Standards and samples (100 µL/well) were
672 incubated for 1 hour at room temperature. After washing four times with wash buffer, 100 µL of
673 biotinylated tracer antibody was added, and the plate was incubated for another hour at room
674 temperature. Following additional washes, 100 µL of streptavidin-peroxidase conjugate was
675 applied, and the plate was incubated for 1 hour. Signal development was performed by adding 100
676 µL of TMB substrate and incubating for 30 minutes in the dark. The reaction was terminated with
677 2% oxalic acid, and absorbance was measured at 450 nm using a microplate reader.

678 Human lactoferrin levels in plasma were measured using the CatchPoint® SimpleStep
679 ELISA® kit (ab229392, Abcam), which employs fluorescence detection. Plasma samples were
680 processed following the manufacturer's recommendations. Standards were prepared by serial
681 dilutions from a reconstituted lactoferrin stock solution. Standards and samples (50 µL each) were
682 added to pre-coated wells, followed by 50 µL of an antibody cocktail containing capture and
683 detector antibodies. Plates were incubated for 1 hour at room temperature on a plate shaker set to
684 400 rpm and subsequently washed three times with Wash Buffer. Detection was performed by
685 adding 100 µL of CatchPoint HRP Development Solution, containing Stoplight Red Substrate and
686 hydrogen peroxide, followed by a 10-minute incubation in the dark. Fluorescence intensity was
687 measured at 530 nm (excitation), 570 nm (cutoff), and 590 nm (emission) using a fluorescence
688 plate reader.

689 Neutrophil extracellular traps (NETs) in plasma samples were quantified using the
690 GENLISA™ Human NETs ELISA Kit (KBH4548, Krishgen BioSystems). Plasma samples were
691 diluted in the Standard Diluent provided. A standard curve was generated using serial dilutions of
692 the NETs standard stock solution. Samples and standards (100 µL each) were added to wells of a
693 microtiter plate pre-coated with anti-NETs antibodies, followed by a 60-minute incubation at
694 37°C. After aspiration, 100 µL of Biotinylated NETs Antibody Working Solution was added, and

695 the plate was incubated for another 60 minutes at 37°C. Wells were then washed four times with
696 1X Wash Buffer to remove unbound components. Next, 100 µL of Streptavidin-HRP Working
697 Solution was added to each well and incubated for 30 minutes at 37°C. Following additional
698 washes, 100 µL of TMB substrate was added to develop the signal during a 10-minute incubation
699 in the dark at 37°C. The reaction was terminated by adding 100 µL of Stop Solution. Absorbance
700 was measured at 450 nm using a microplate reader within 15 minutes of adding the Stop Solution.
701 A standard curve was generated by plotting absorbance or fluorescence values against
702 known analyte concentrations, and sample concentrations were interpolated and adjusted for
703 dilution factors. Background correction was performed by subtracting the blank (zero standard)
704 signal from all optical density (OD) or fluorescence values. Samples exceeding the upper limit of
705 quantification were reanalyzed at higher serum dilutions when possible; otherwise, data was
706 analyzed as background-corrected OD or fluorescence values. All assays were conducted in
707 duplicate, and results were reported as the mean of the technical replicates. Outliers were identified
708 and removed using the Interquartile Range (IQR) method. Boundaries for identifying outliers were
709 defined as follows: Lower Bound: Q1 – (1.5 × IQR); Upper Bound: Q3 + (1.5 × IQR).
710 Observations with values outside these thresholds were considered outliers and excluded from
711 further analysis.
712
713 Statistical analysis

714 All statistical analyses were performed using R (v4.2.3, R Foundation for Statistical Computing).
715 Differences in the ED_{50} of binding antibodies in pre-infection samples between children who
716 subsequently experienced DF or DHF/DSS were analyzed using a two-tailed Wilcoxon rank-sum
717 test with false discovery rate (FDR) correction for multiple comparisons. Logistic regression
718 models were employed to evaluate the association between pre-existing antibody profiles and the
719 subsequent development of DHF/DSS. Each antibody characteristic was analyzed in a separate
720 regression model, with FDR correction applied for multiple hypothesis testing.
721 To adjust the coefficients of the antibody characteristics correlated with DHF/DSS, we
722 performed a multivariate regression with regularization. To estimate the regularization parameters,
723 the dataset was divided into training and testing sets (50-50 split). Optimal regularization
724 parameters (gamma and alpha) were determined via bootstrapping (n=1000), maximizing the area
725 under the curve (AUC) on the training set. Then, the optimal parameters were applied to re-

726 estimate the coefficients for selected antibody features using the entire dataset. Regularization was
727 implemented using the glmnet R package (v4.1-860).

728 To compare the predictive accuracy of Total IgA versus Total IgG antibody avidity in pre-
729 infection samples for distinguishing the children who subsequently developed DF or DHF/DSS, a
730 similar regularization approach was used. In addition, the variables in the final model were
731 assessed using an orthogonal partial least squares discriminant analysis (OPLS-DA) to estimate
732 the variance in the response variable explained by the model (R^2Y), the predictive performance for
733 new data (Q^2), and the overall classification accuracy. Two models were compared: avidity of IgA
734 antibodies alone, and avidity of IgG antibodies alone.

735 Normalized phagocytic scores, percentage changes in signal in the NETosis assay, relative
736 neutrophil counts, and levels of degranulation markers were compared across clinical groups using
737 a one-tailed Wilcoxon rank-sum test. Logistic regression was employed to assess the association
738 between degranulation marker levels and severe disease manifestations, estimating odds ratios
739 (ORs) and 95% confidence intervals (CIs) using the oddsratio package (v2.0.1). Linear regression
740 was used to evaluate the relationships between degranulation markers and antibody binding
741 profiles, as well as between degranulation markers and maximum gallbladder wall thickness. All
742 statistical analyses were conducted at a significance level of 5%.
743

744 **References**

745

746 1. Bhatt, S. *et al.* The global distribution and burden of dengue. *Nature* **496**, 504–507 (2013).

747 2. Paz-Bailey, G., Adams, L. E., Deen, J., Anderson, K. B. & Katzelnick, L. C. Dengue. *The*
748 *Lancet* **403**, 667–682 (2024).

749 3. Katzelnick, L. C. *et al.* Antibody-dependent enhancement of severe dengue disease in
750 humans. *Science (1979)* **358**, 929–932 (2017).

751 4. Katzelnick, L. C. *et al.* Zika virus infection enhances future risk of severe dengue disease.
752 *Science (1979)* **369**, 1123–1128 (2020).

753 5. Zambrana, J. V. *et al.* Primary exposure to Zika virus is linked with increased risk of
754 symptomatic dengue virus infection with serotypes 2, 3, and 4, but not 1. *Sci Transl Med*
755 **16**, 2199 (2024).

756 6. Estofolete, C. F. *et al.* Influence of previous Zika virus infection on acute dengue episode.
757 *PLoS Negl Trop Dis* **17**, e0011710 (2023).

758 7. Yamanaka, A. *et al.* Antibody-dependent enhancement representing in vitro infective
759 progeny virus titer correlates with the viremia level in dengue patients. *Sci Rep* **11**, (2021).

760 8. Waggoner, J. J. *et al.* Antibody-Dependent Enhancement of Severe Disease Is Mediated by
761 Serum Viral Load in Pediatric Dengue Virus Infections. *J Infect Dis* **221**, 1846–1854
762 (2020).

763 9. Bournazos, S. *et al.* Antibody fucosylation predicts disease severity in secondary dengue
764 infection. *Science (1979)* **372**, 1102–1105 (2021).

765 10. Yamin, R. *et al.* Human FcγRIIIa activation on splenic macrophages drives dengue
766 pathogenesis in mice. *Nat Microbiol* **8**, 1468–1479 (2023).

767 11. Gordon, A. *et al.* The Nicaraguan Pediatric Dengue Cohort Study: Incidence of Inapparent
768 and Symptomatic Dengue Virus Infections, 2004–2010. *PLoS Negl Trop Dis* **7**, e2462
769 (2013).

770 12. Bos, S. *et al.* Serotype-specific epidemiological patterns of inapparent versus symptomatic
771 primary dengue virus infections: a 17-year cohort study in Nicaragua. *Lancet Infect Dis*
772 (2024) doi:10.1016/S1473-3099(24)00566-8.

773 13. Perciani, C. T., Peixoto, P. S., Dias, W. O., Kubrusly, F. S. & Tanizaki, M. M. Improved
774 method to calculate the antibody avidity index. *J Clin Lab Anal* **21**, 201–206 (2007).

775 14. Shackelford, P. G., Granoff, D. M., Madassery, J. V, Scott, M. G. & Nahm, M. H. Clinical
776 and Immunologic Characteristics of Healthy Children with Subnormal Serum
777 Concentrations of IgG2. *Pediatr Res* **27**, 16–21 (1990).
778 15. Plebani, A. *et al.* Serum IgG subclass concentrations in healthy subjects at different age:
779 Age normal percentile charts. *Eur J Pediatr* **149**, 164–167 (1989).
780 16. Steffen, U. *et al.* IgA subclasses have different effector functions associated with distinct
781 glycosylation profiles. *Nat Commun* **11**, 120 (2020).
782 17. Mayer-Hain, S. *et al.* Systemic Activation of Neutrophils by Immune Complexes Is Critical
783 to IgA Vasculitis. *J Immun* **209**, 1048–1058 (2022).
784 18. Pillebout, E. IgA Vasculitis and IgA Nephropathy: Same Disease? *J Clin Med* **10**, 2310
785 (2021).
786 19. Aroca-Crevillén, A., Vicanolo, T., Ovadia, S. & Hidalgo, A. Neutrophils in Physiology and
787 Pathology. *Annu Rev Pathol* **19**, 227–259 (2024).
788 20. Dias, A. G. *et al.* Antibody Fc characteristics and effector functions correlate with protection
789 from symptomatic dengue virus type 3 infection. *Sci Transl Med* **14**, 3151 (2022).
790 21. Strich, J. R. *et al.* Fostamatinib Inhibits Neutrophils Extracellular Traps Induced by
791 COVID-19 Patient Plasma: A Potential Therapeutic. *J Infect Dis* **223**, 981–984 (2021).
792 22. Narvaez, F. *et al.* Dengue severity by serotype and immune status in 19 years of pediatric
793 clinical studies in Nicaragua. *PLoS Negl Trop Dis* **19**, e0012811 (2025).
794 23. Colbert, J. A. *et al.* Ultrasound measurement of gallbladder wall thickening as a diagnostic
795 test and prognostic indicator for severe dengue in pediatric patients. *Pediatr Infect Dis J* **26**,
796 850–852 (2007).
797 24. Ferreira, B. D. C. & Correia, D. Ultrasound Assessment of Hepatobiliary and Splenic
798 Changes in Patients With Dengue and Warning Signs During the Acute and Recovery
799 Phases. *J Ultrasound Med* **38**, 2015–2024 (2019).
800 25. Srikiatkhachorn, A. *et al.* Natural History of Plasma Leakage in Dengue Hemorrhagic
801 Fever. *Pediatr Infect Dis J* **26**, 283–290 (2007).
802 26. Ruchusatsawat, K. *et al.* Long-term circulation of Zika virus in Thailand: an observational
803 study. *Lancet Infect Dis* **19**, 439–446 (2019).
804 27. Monteiro, R. C. & Suzuki, Y. Are there animal models of IgA nephropathy? *Semin*
805 *Immunopathol* **43**, 639–648 (2021).

806 28. Seminario, G. *et al.* The Latin American Society for Immunodeficiencies Registry. *J Clin*
807 *Immunol* **45**, 28 (2024).
808 29. Wang, Z. *et al.* Enhanced SARS-CoV-2 neutralization by dimeric IgA. *Sci Transl Med* **13**,
809 1555 (2021).
810 30. Wegman, A. D. *et al.* DENV-specific IgA contributes protective and non-pathologic
811 function during antibody-dependent enhancement of DENV infection. *PLoS Pathog* **19**,
812 e1011616 (2023).
813 31. Upadhaya, B. K. *et al.* Transient IgA nephropathy with acute kidney injury in a patient with
814 dengue fever. *Saudi J Kidney Dis Transpl* **21**, 521–5 (2010).
815 32. Bachal, R. *et al.* Higher levels of dengue-virus-specific IgG and IgA during pre-
816 defervescence associated with primary dengue hemorrhagic fever. *Arch Virol* **160**, 2435–
817 2443 (2015).
818 33. Chia, P. Y., Teo, A. & Yeo, T. W. Association of Neutrophil Mediators with Dengue
819 Disease Severity and Cardiac Impairment in Adults. *J Infect Dis* **226**, 1974–1984 (2022).
820 34. Loke, P. *et al.* Gene Expression Patterns of Dengue Virus-Infected Children from Nicaragua
821 Reveal a Distinct Signature of Increased Metabolism. *PLoS Negl Trop Dis* **4**, e710 (2010).
822 35. Recker, M. *et al.* Markers of prolonged hospitalisation in severe dengue. *PLoS Negl Trop*
823 *Dis* **18**, e0011922 (2024).
824 36. Robinson, M. *et al.* A 20-Gene Set Predictive of Progression to Severe Dengue. *Cell Rep*
825 **26**, 1104-1111.e4 (2019).
826 37. Liu, Y. E. *et al.* An 8-gene machine learning model improves clinical prediction of severe
827 dengue progression. *Genome Med* **14**, 33 (2022).
828 38. Duggal, S. *et al.* Dengue virus infection in mice induces bone marrow myeloid cell
829 differentiation and generates Ly6Glow immature neutrophils with modulated functions. *J*
830 *Leukoc Biol* **115**, 130–148 (2024).
831 39. Stacey, H. D. *et al.* IgA potentiates NETosis in response to viral infection. *Proc Natl Acad*
832 *Sci U S A* **118**, (2021).
833 40. Gimpel, A.-K. *et al.* IgA Complexes Induce Neutrophil Extracellular Trap Formation More
834 Potently Than IgG Complexes. *Front Immunol* **12**, 761816 (2021).
835 41. Knackstedt, S. L. *et al.* Neutrophil extracellular traps drive inflammatory pathogenesis in
836 malaria. *Sci Immunol* **4**, 336 (2019).

837 42. Passelli, K. *et al.* The c-MET receptor tyrosine kinase contributes to neutrophil-driven
838 pathology in cutaneous leishmaniasis. *PLoS Pathog* **18**, e1010247 (2022).
839 43. Biering, S. B. *et al.* Structural basis for antibody inhibition of flavivirus NS1–triggered
840 endothelial dysfunction. *Science (1979)* **371**, 194–200 (2021).
841 44. Modhiran, N. *et al.* A broadly protective antibody that targets the flavivirus NS1 protein.
842 *Science (1979)* **371**, 190–194 (2021).
843 45. Németh, T., Sperandio, M. & Mócsai, A. Neutrophils as emerging therapeutic targets. *Nat*
844 *Rev Drug Discov* **19**, 253–275 (2020).
845 46. Gordon, A. *et al.* The Nicaraguan pediatric influenza cohort study: design, methods, use of
846 technology, and compliance. *BMC Infect Dis* **15**, 504 (2015).
847 47. Narvaez, F. *et al.* Evaluation of the Traditional and Revised WHO Classifications of Dengue
848 Disease Severity. *PLoS Negl Trop Dis* **5**, e1397 (2011).
849 48. Balmaseda, A. *et al.* Comparison of Four Serological Methods and Two Reverse
850 Transcription-PCR Assays for Diagnosis and Surveillance of Zika Virus Infection. *J Clin*
851 *Microbiol* **56**, e01785-17 (2018).
852 49. Waggoner, J. J. *et al.* Single-Reaction, Multiplex, Real-Time RT-PCR for the Detection,
853 Quantitation, and Serotyping of Dengue Viruses. *PLoS Negl Trop Dis* **7**, e2116 (2013).
854 50. Waggoner, J. J. *et al.* Single-Reaction Multiplex Reverse Transcription PCR for Detection
855 of Zika, Chikungunya, and Dengue Viruses. *Emerg Infect Dis* **22**, 1295–1297 (2016).
856 51. Gordon, A. *et al.* Prior dengue virus infection and risk of Zika: A pediatric cohort in
857 Nicaragua. *PLoS Med* **16**, e1002726 (2019).
858 52. Cohen, J. *Statistical Power Analysis for the Behavioral Sciences*. (Lawrence Erlbaum
859 Associates, 2013).
860 53. Johnson, B. W., Russell, B. J. & Lanciotti, R. S. Serotype-Specific Detection of Dengue
861 Viruses in a Fourplex Real-Time Reverse Transcriptase PCR Assay. *J Clin Microbiol* **43**,
862 4977–4983 (2005).
863 54. Dias, A. G. *et al.* Complement-dependent virion lysis mediated by dengue-Zika virus cross-
864 reactive antibodies correlates with protection from severe dengue disease. *Cell Rep* In Press
865 (2025) doi:10.1101/2024.06.03.24308395.
866 55. Kudlacek, S. T. *et al.* Designed, highly expressing, thermostable dengue virus 2 envelope
867 protein dimers elicit quaternary epitope antibodies. *Sci Adv* **7**, 4084–4099 (2021).

868

869 **Acknowledgments:** We thank the study personnel at the Centro de Salud Sócrates Flores Vivas,
870 the Nicaraguan National Virology Laboratory, the Hospital Infantil Manuel de Jesús Rivera, and
871 the Sustainable Sciences Institute in Nicaragua. We are particularly grateful to the study
872 participants and their families. We would also like to thank Olivia Cuaresma for her technical
873 support, Myha Hill for support in code development, and Dr. Jeffrey R. Strich and Kiana Allen for
874 their contributions to prior development of the NETosis assay.

875

876 **Funding:** This work was supported by NIH/NIAID grants P01AI106695 (EH) and U01AI153416
877 (EH). The Nicaraguan cohort and hospital studies were supported by NIH/NIAID grants
878 U19AI118610 (EH), R01 AI099631 (AB), P01AI106695 (EH), and U01AI153416 (EH). MJRB
879 is supported by funding from the Research Centers in Minority Institutions (RCMI) Center for
880 Research Resources Grant and the Molecular and Genomics Core (U54MD007579) and the
881 Hispanic Alliance for Clinical and Translational Research - Mentor Mentee Program Grant
882 (5U54GM133807-03)

883

884 **Author contributions:**

885 Conceptualization: JACO, EH

886 Methodology: JACO, EH, SB, JVZ, VR, BB, MJRB, GA, KA

887 Investigation: JACO, ED, AB, DEMJ, VR, BB, JZ, JH, AGD, KA

888 Visualization: JACO

889 Funding acquisition: EH, GA, MJRB

890 Project administration: EH

891 Supervision: EH

892 Writing – original draft: JACO, EH

893 Writing – review & editing: JACO, EH, SB, JVZ, AGD, VR, AB, MJRB, DEMJ, GA, JZ, JH, KA

894

895 **Competing interests:** EH's laboratory received research funds from Takeda Vaccines Inc. to test
896 samples from vaccine recipients. EH served on one-time advisory boards for Merck and Takeda.
897 G.A. was an employee of Moderna Therapeutics and holds equity in Leyden Labs and Systems
898 Seromyx. The other authors declare that they have no competing interests.
899
900 **Data and materials availability:** All data associated with this study are present in the main text
901 or supplementary materials. The associated code is available for reference on Zenodo. Reference
902 code and datasets for antibody profiling and coefficient adjustment using regularization (DOI:
903 10.5281/zenodo.14837883), reference code for assessing the classification performance of IgA,
904 IgG, and IgG/IgA avidity (DOI: 10.5281/zenodo.14837889), and source data for figures (DOI:
905 10.5281/zenodo.14837915). After securing approval from the UC Berkeley Committee for the
906 Protection of Human Subjects, individual data for figure reproduction can be shared with external
907 researchers. For data access arrangements, please contact E.H. at eharris@berkeley.edu. Standard
908 data and material transfer agreements govern all data used in this study.
909

910 **Supplementary Materials**

911 Figs. S1 to S5

912 Table S1

913

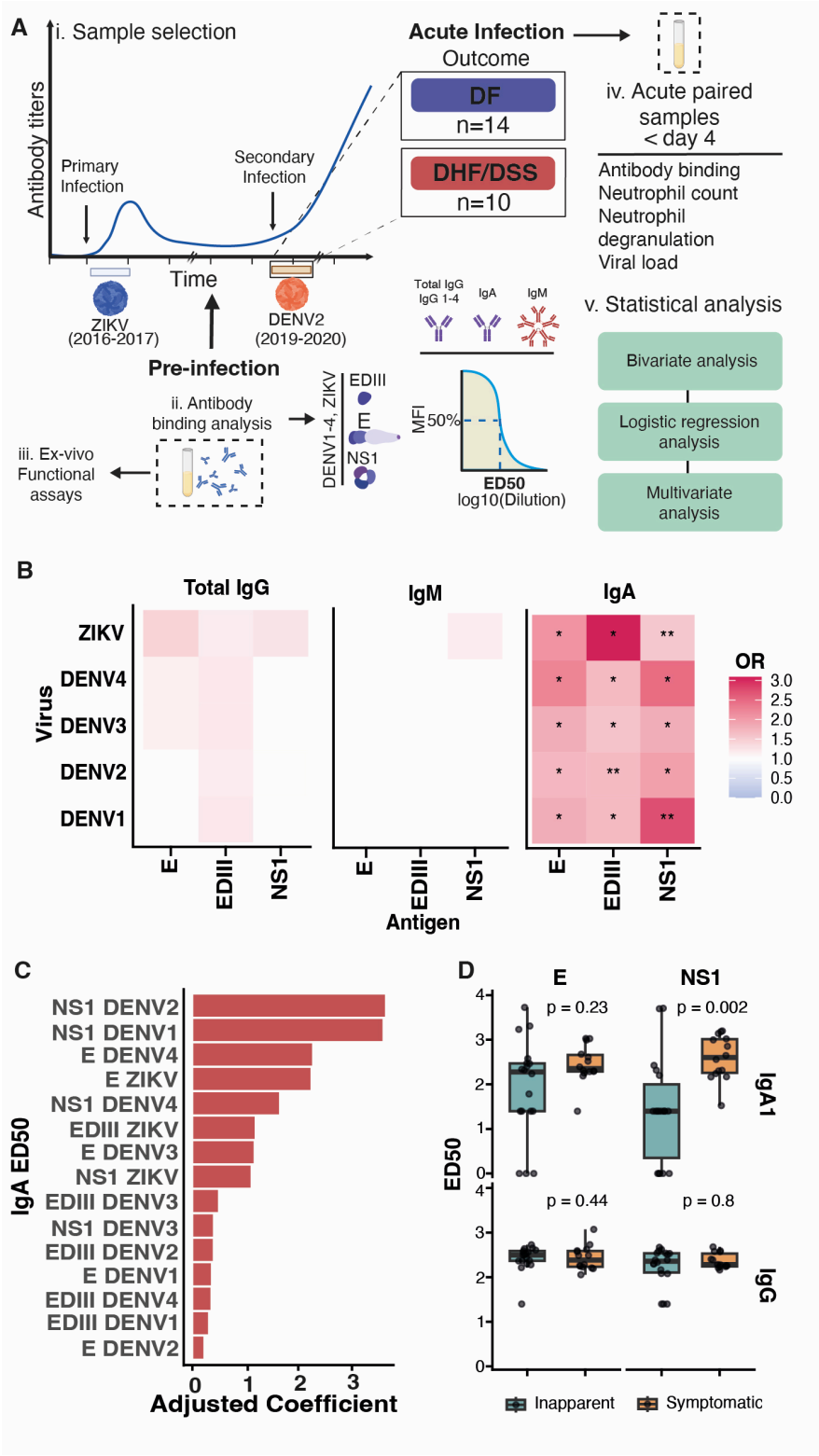

914

915 **Fig 1. Study design and antibody profiling of post-ZIKV DENV2 cases in the Pediatric**
916 **Dengue Cohort Study.** (**A**) Study workflow. (i) Sample selection: plasma samples from children
917 with primary ZIKV infection (2016) who developed dengue fever (DF, n=14) or dengue

hemorrhagic fever/dengue shock syndrome (DHF/DSS, n=10) during a subsequent DENV2 infection (2019–2020) were analyzed. (ii) Antibody binding analysis was performed in pre-infection samples (after the primary ZIKV infection and before the subsequent DENV2 infection). (iii) *Ex vivo* functional assays with pre-infection antibodies were performed to analyze neutrophil activation, and (iv) neutrophil involvement during acute infection was assessed using paired acute-phase samples. (v) The statistical approach involved bivariate and multivariate analysis. (**B**) Heatmaps display the odds ratio of developing DHF/DSS for IgG, IgM, and IgA binding to the antigens tested. Significance: *$p<0.05$, **$p<0.01$ after False Discovery Rate (FDR) correction. (**C**) Adjusted coefficients via regularization reveal NS1 DENV2 binding as the strongest predictor of disease severity. (**D**) Comparison of ED_{50} values for IgA1 and IgG binding to E and NS1 antigens following primary ZIKV infection and prior to subsequent DENV2 infection, stratified by inapparent versus symptomatic outcomes. Boxplots show the median, interquartile range, and whiskers extending to 1.5× the interquartile range; individual dots represent participant values. Statistical comparisons were performed using one-tailed Wilcoxon rank-sum tests.

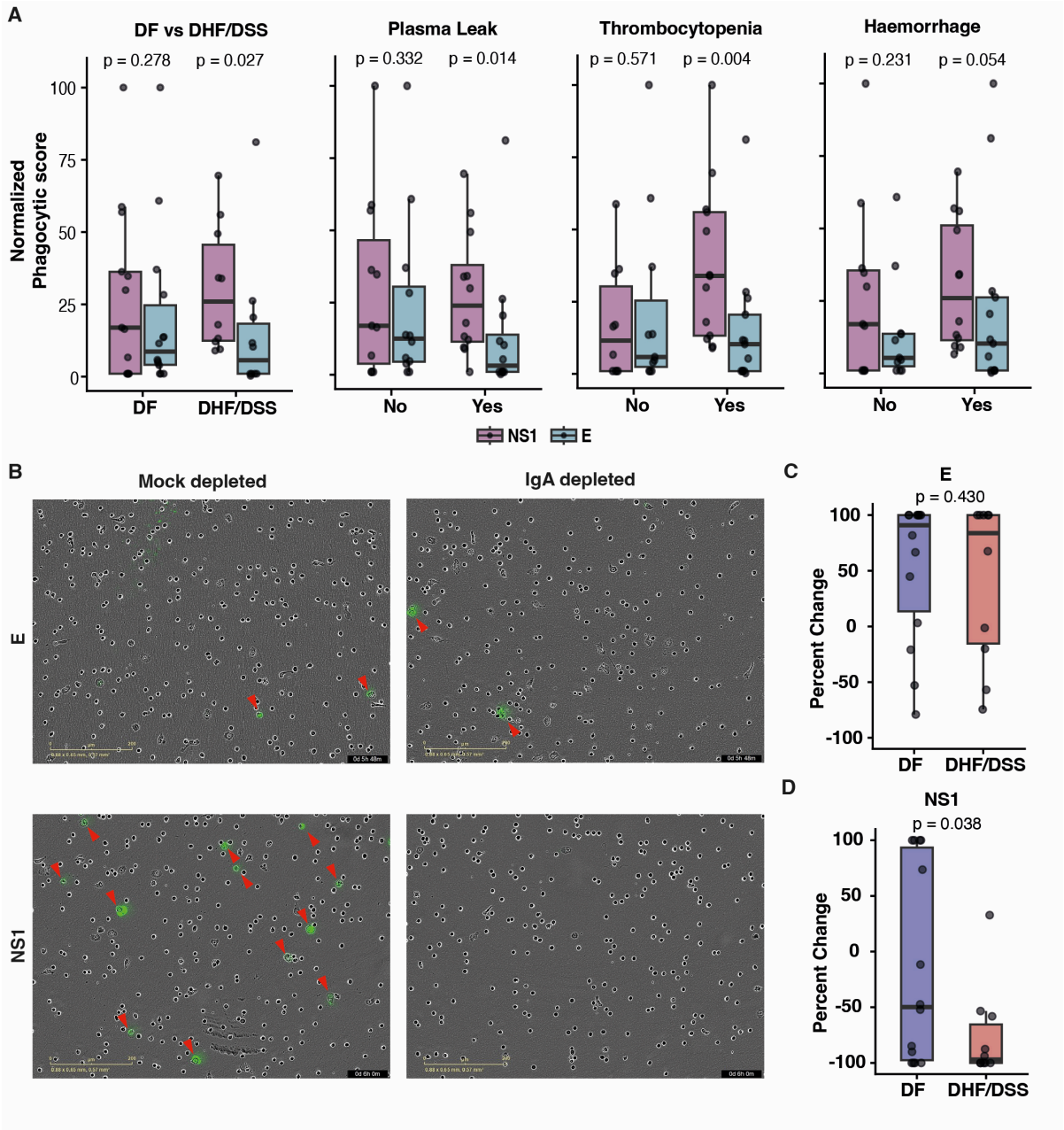

Fig. 2. IgA antibodies targeting NS1 induce enhanced neutrophil activation in DHF/DSS cases. (**A**) Antibody-dependent neutrophil phagocytosis (ADNP) normalized phagocytic scores across clinical groups and severe disease manifestations. Data points represent the average of two replicates from two different healthy donors per sample (DF=14, DHF/DSS=10). Pre-infection plasma from children that subsequently developed DHF/DSS, thrombocytopenia, or plasma leakage exhibited significantly higher ADNP against NS1 compared to E, particularly in association with plasma leakage (p=0.014) and thrombocytopenia (p=0.004). The data indicate a skewed neutrophil activation response toward NS1 in severe cases. (**B**) Representative microscopy images of NETosis assays. Panels compare mock-depleted plasma (left) and IgA-depleted plasma (right) for E (upper) and NS1 (lower) antigens. IgA depletion significantly reduces NET formation

957 in NS1-coated wells (p=0.038), highlighting the role of IgA in mediating neutrophil activation.
958 Red arrows indicate NETs. Scale bar=200 µm. (**C**, **D**) Quantification of percent change in NETosis
959 signal for E (**C**) and NS1 (**D**) antigens after IgA depletion. Data points represent the percent change
960 comparing paired depleted and mock-depleted samples from participants who developed DF
961 (n=14) or DHF/DSS (n=10). While no significant difference was observed for E, NETosis was
962 significantly reduced in DHF/DSS cases when NS1-specific IgA was depleted. Statistical
963 comparisons were performed using one-tailed Wilcoxon rank-sum tests.

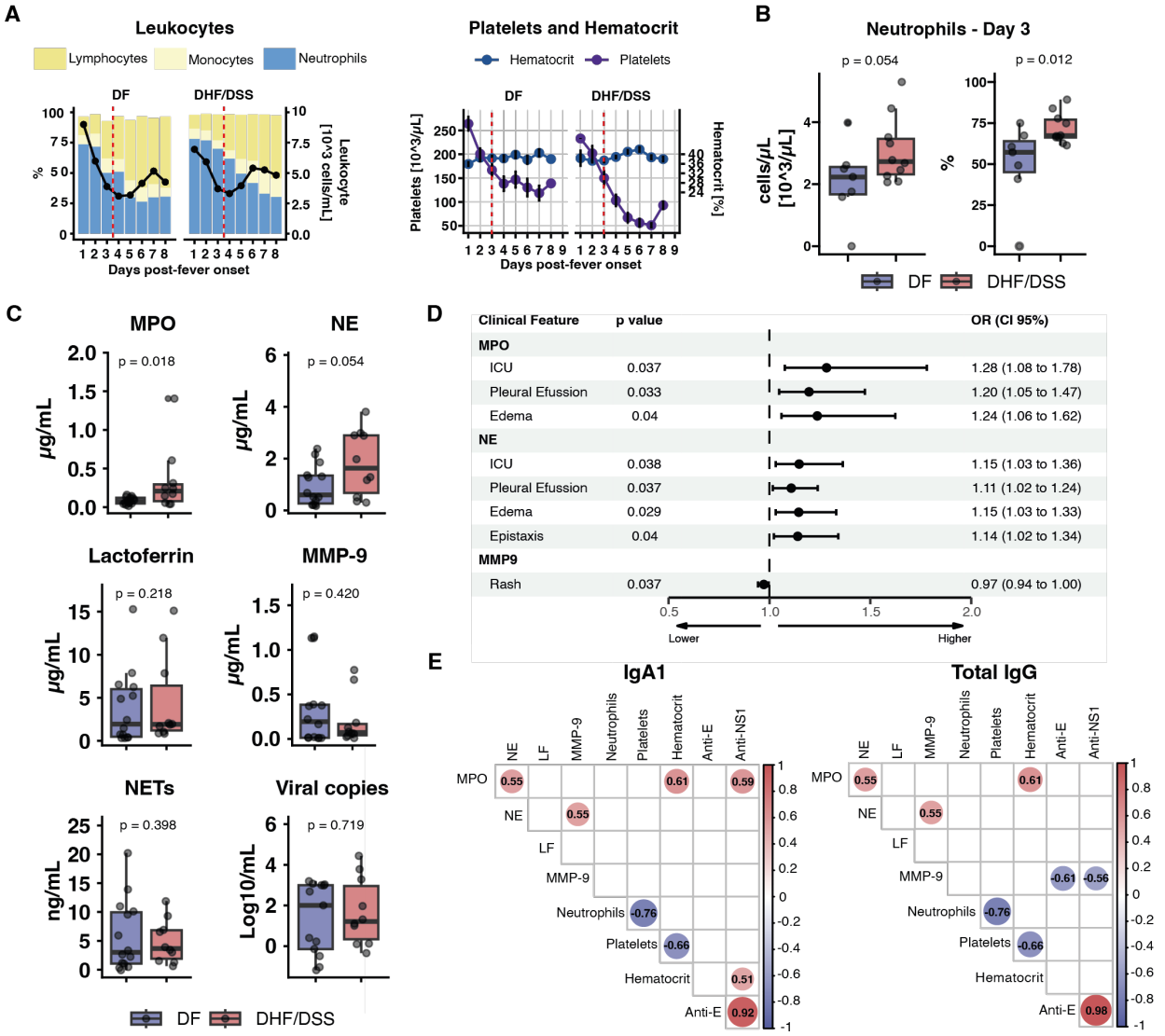

Fig 3. Enhanced neutrophil activation during acute DENV2 infection correlates with disease severity and binding of anti-NS1 IgA1 antibodies. (**A**) Relative leukocyte proportions (left panel), platelet counts, and hematocrit levels (right panel) in DF and DHF/DSS cases over time. Day 3 post-fever onset is marked with a dashed red line. The dark line corresponds to leukocyte count (units displayed on the right axis). (**B**) Neutrophil counts on day 3 post-fever onset—prior to the onset of thrombocytopenia (platelet count<100,000/μL)—were significantly elevated in children who progressed to DHF/DSS (p=0.012). Left panel: Absolute neutrophil count, Right panel: Relative neutrophil count. (**C**) Levels of primary granule markers (myeloperoxidase [MPO], neutrophil elastase [NE]), secondary granule markers (lactoferrin), tertiary granule markers (MMP-9), NETs, and viral loads among children with DF or DHF/DSS. DHF/DSS cases displayed higher levels of MPO (p=0.018) and NE (p=0.054), with no significant difference in viral load. In

988 all boxplots, boxes represent the interquartile range (IQR) with median values shown as horizontal
989 lines; whiskers extend to 1.5×IQR; individual points represent participants. Statistical comparisons
990 were performed using one-tailed Wilcoxon rank-sum tests. (**D**) Logistic regression shows
991 significant correlation between MPO, NE, and severe outcomes such as ICU admission and pleural
992 effusion (OR with 95% CI). (**E**) Correlation heatmaps between antibody binding, neutrophil
993 degranulation and clinical parameters of disease severity. Circle color indicates the direction of
994 the correlation (red, positive; blue, negative), the circle size is proportional to the magnitude of the
995 Pearson correlation coefficient, and the coefficient is displayed inside each circle. Only significant
996 correlations (adjusted p-value<0.05) after FDR correction are displayed. IgA1 binding to NS1
997 positively correlates with MPO, while IgG inversely correlates with MMP-9. Anti-NS1 IgA1
998 positively correlates with hematocrit.
999

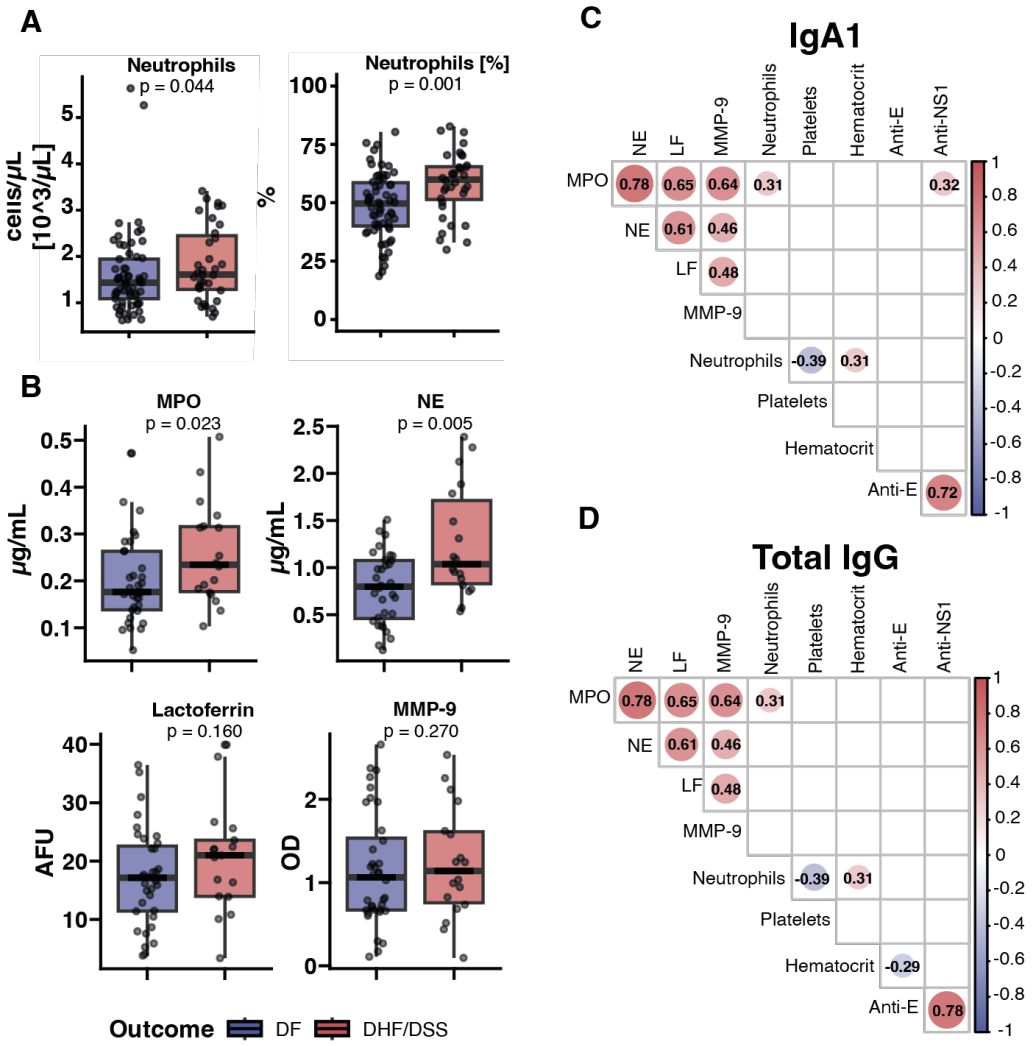

Fig. 4. Neutrophil degranulation correlates with anti-NS1 IgA1 antibodies in an orthogonal hospital-based study. (**A**) Boxplots show the absolute count (left) and percentage (right) of circulating neutrophils in dengue fever (DF) and dengue hemorrhagic fever/dengue shock syndrome (DHF/DSS) cases. DHF/DSS was characterized by increased absolute (cells/uL) and relative (%) neutrophil counts. (**B**) Boxplots display plasma concentrations of neutrophil activation markers [myeloperoxidase (MPO), neutrophil elastase (NE), lactoferrin (LF), and matrix metalloproteinase 9 (MMP-9)] during acute DENV2 infection in each clinical group. In all boxplots, boxes represent the interquartile range (IQR) with median values shown as horizontal lines; whiskers extend to 1.5×IQR; individual points represent participants; p-values were calculated using one-tailed Wilcoxon's rank-sum test. Participants who developed DHF/DSS had higher levels of primary granule components (MPO and NE). (**C, D**) Correlation of neutrophil relative counts, neutrophil degranulation and antibody binding with anti-NS1 and anti-E IgA1

1013 antibodies (**C**) and Total IgG antibodies (**D**). Correlation heatmaps show pairwise Spearman's
1014 correlation coefficients. Only significant correlations (p-value<0.05) are displayed. Circle color
1015 indicates correlation direction (red, positive; blue, negative), circle size is proportional to the
1016 absolute correlation coefficient, and the coefficient value is displayed within each circle. Anti-NS1
1017 IgA1 antibodies correlate with increased MPO. Anti-E IgG negatively correlate with hematocrit.
1018

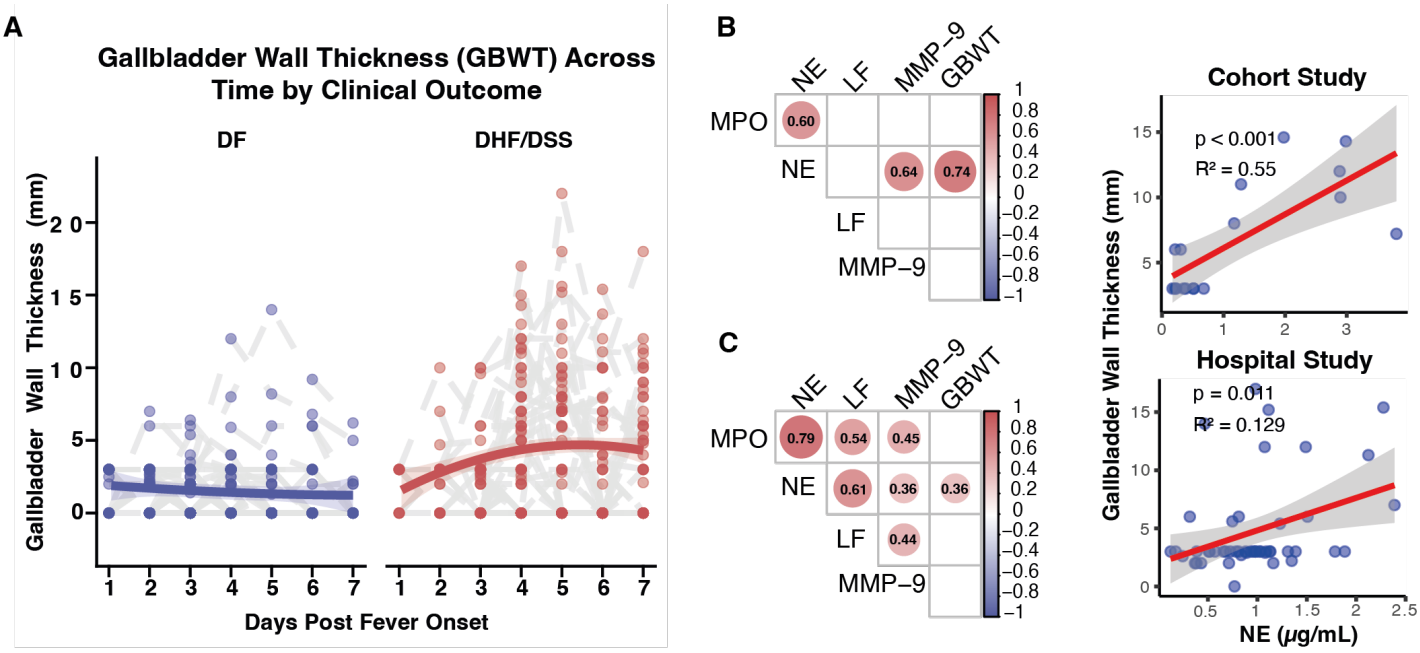

Fig. 5. Neutrophil activation precedes and correlates with vascular leakage during acute DENV2 infection across two independent studies. (**A**) Gallbladder wall thickness (GBWT) over time in DF and DHF/DSS cases in the PDHS and PDCS. Greater gallbladder wall thickness was observed in DHF/DSS cases during acute infection, reflecting increased vascular leakage. (**B**, **C**) Correlation analyses between neutrophil degranulation and gallbladder thickness in the PDCS (**B**) and PDHS (**C**). Correlation heatmaps show pairwise Pearson's correlation coefficients. Only significant correlations (p-value<0.05) are displayed. Circle color indicates correlation direction (red, positive; blue, negative), circle size is proportional to the absolute correlation coefficient, and the coefficient value is displayed within each circle. A positive correlation is observed between NE levels (measured on/before day 3 post-fever onset) and maximum gallbladder wall thickness in the PDCS ($p<0.001$, $R^2=0.55$) and PDHS ($p=0.01$, $R^2=0.129$).

1039 **Extended Data Figure 1. Antibody binding profile of pre-infection plasma of children after**
1040 **a primary ZIKV infection and before subsequent DENV2 disease. (A)** Antibody binding
1041 profiles for E, EDIII, and NS1 antigens from DENV1-4 and ZIKV in plasma prior to dengue fever
1042 (DF = 14) or dengue hemorrhagic fever/dengue shock syndrome (DHF/DSS = 10) cases. Binding
1043 levels (ED_{50}) are shown for total IgG, IgG1-4 subclasses, IgM, and total IgA in a $\log_{10}$ scale.
1044 DHF/DSS cases consistently displayed significantly higher IgA binding levels across all DENV
1045 serotypes and antigens compared to DF cases. Statistical comparisons were performed using two-
1046 tailed Wilcoxon rank-sum tests and p values were adjusted by multiple comparisons. False
1047 discovery rate (FDR)-adjusted p-values are shown above the plots for significant associations.
1048
1049 **Extended Data Figure 2. Antibody avidity of IgA and IgG antibodies against E, EDIII, and**
1050 **NS1, and multivariate discrimination of clinical outcomes.** A) Boxplots show avidity indices
1051 of IgA (top) and IgG (bottom) binding to E, NS1, and EDIII antigens from DENV1–4 and ZIKV
1052 in dengue fever (DF) and dengue hemorrhagic fever/dengue shock syndrome (DHF/DSS) cases.
1053 Boxes represent the interquartile range (IQR) with medians indicated by horizontal lines; whiskers
1054 extend to 1.5×IQR; individual dots represent participants. Avidity was assessed by comparing
1055 antigen binding after exposure to 7 M urea (chaotropic agent) versus PBS. Statistical comparisons
1056 were performed using two-tailed Wilcoxon rank-sum tests and p values were adjusted by multiple
1057 comparisons. No significant associations were identified between groups. (**B**) Orthogonal partial
1058 least squares discriminant analysis (OPLS-DA) of avidity features distinguishes DF (blue) from
1059 DHF/DSS (red) cases. Left: Total IgA avidity predicted clinical outcome (Accuracy = 0.92, 95%
1060 CI: 0.62–1.0, p = 0.015; $R^2Y = 0.715$; p = 0.004; $Q^2 = 0.473$; p = 0.002), whereas total IgG avidity
1061 did not (Accuracy = 0.5, 95% CI: 0.21–0.79, p = 0.811; $R^2Y = 0.291$, p = 0.276; $Q^2 = -0.14$, p =
1062 0.379).

1063 **Extended Data Figure 3. Antibody-dependent neutrophil phagocytosis (ADNP) mediated by**
1064 **pre-infection antibodies.** (**A**) Coupling efficiency of biotinylated E and NS1 proteins to
1065 streptavidin-coated beads. Coupling density was quantified by probing with anti-biotin-PE and
1066 measuring median fluorescence intensity (MFI). Bars represent mean log10 (MFI) ± 95% CI from
1067 six independent replicates, showing comparable coupling efficiency of E and NS1. (**B**) Normalized
1068 ADNP scores for NS1 and E elicited by pre-infection plasma from DF (n = 14) and DHF/DSS (n
1069 = 10) cases. Pre-infection antibodies from children who later developed thrombocytopenia induced
1070 significantly higher ADNP against NS1. Data points represent the average of two replicates across
1071 two independent healthy donors per sample. (**C**) Spearman correlation heatmap showing
1072 associations between ADNP (NS1 or E) and clinical parameters (minimum platelet count,
1073 maximum hematocrit). Circle color indicates correlation direction (red, positive; blue, negative);
1074 size and intensity reflect magnitude. Only significant correlations are displayed ($p<0.05$). ADNP
1075 to NS1 was positively correlated with higher hematocrit during subsequent DENV2 infection. (**D**)
1076 Spearman's correlation between ADNP to NS1 or E and the avidity index (AI) of IgA and IgG
1077 against the corresponding antigens. Only NS1-specific IgA avidity was significantly associated
1078 with ADNP to NS1. Adjusted p values after false discovery rate correction are shown.

1079 **Extended Data Figure 4. Neutrophil activation and functional ex vivo responses to E and**
1080 **NS1 antigens in the presence of pre-infection antibodies**. Representative images of NETosis
1081 assays. Neutrophils were incubated with medium alone (negative control) or phorbol 12-myristate

1082 13-acetate (PMA; positive control) in the presence of E or NS1 antigens. Green fluorescence
1083 indicates extracellular DNA release characteristic of NET formation. Scale bars: 200 µm.

1084 **Extended Data Figure 5. Longitudinal dynamics of leukocyte populations, platelets and**
1085 **hematocrit in the Pediatric Dengue Hospital-based Study (PDHS) and correlations between**
1086 **degranulation markers and gallbladder wall thickness in the Pediatric Dengue Cohort Study**
1087 **(PDCS) and PDHS. (A)** Temporal dynamics of leukocyte populations (lymphocytes, monocytes,
1088 and neutrophils) in DF and DHF/DSS cases (left panel). The dashed red line marks the cutoff of
1089 normal leukocyte counts. Platelet counts and hematocrit trajectories during acute infection are
1090 shown (right panel) in the PDHS. **(B)** Pearson's correlation analysis in the PDCS between
1091 gallbladder wall thickness and neutrophil degranulation markers, including myeloperoxidase
1092 (MPO), lactoferrin, and matrix metalloproteinase-9 (MMP-9). Raw p-values (non adjusted by
1093 multiple comparison) are displayed. MPO showed a significant positive correlation with
1094 gallbladder wall thickness ($p = 0.030$, $R^2 = 0.276$). **(C)** Correlation analysis in the PDHS between
1095 gallbladder wall thickness and neutrophil degranulation markers.

1096